
Large-Scale Differentiable Causal Discovery of Factor Graphs

Romain Lopez^{1,2}, Jan-Christian Hütter¹,
Jonathan K. Pritchard^{2,3,†}, Aviv Regev^{1,†}

¹ Division of Research and Early Development, Genentech
{lopez.romain, huettej1, regeva}@gene.com

² Department of Genetics, Stanford University
pritch@stanford.edu

³ Department of Biology, Stanford University

† These authors contributed equally to this work.

Abstract

A common theme in causal inference is learning causal relationships between observed variables, also known as causal discovery. This is usually a daunting task, given the large number of candidate causal graphs and the combinatorial nature of the search space. Perhaps for this reason, most research has so far focused on relatively small causal graphs, with up to hundreds of nodes. However, recent advances in fields like biology enable generating experimental data sets with thousands of interventions followed by rich profiling of thousands of variables, raising the opportunity and urgent need for large causal graph models. Here, we introduce the notion of factor directed acyclic graphs (f -DAGs) as a way to restrict the search space to non-linear low-rank causal interaction models. Combining this novel structural assumption with recent advances that bridge the gap between causal discovery and continuous optimization, we achieve causal discovery on thousands of variables. Additionally, as a model for the impact of statistical noise on this estimation procedure, we study a model of edge perturbations of the f -DAG skeleton based on random graphs and quantify the effect of such perturbations on the f -DAG rank. This theoretical analysis suggests that the set of candidate f -DAGs is much smaller than the whole DAG space and thus may be more suitable as a search space in the high-dimensional regime where the underlying skeleton is hard to assess. We propose Differentiable Causal Discovery of Factor Graphs (DCD-FG), a scalable implementation of f -DAG constrained causal discovery for high-dimensional interventional data. DCD-FG uses a Gaussian non-linear low-rank structural equation model and shows significant improvements compared to state-of-the-art methods in both simulations as well as a recent large-scale single-cell RNA sequencing data set with hundreds of genetic interventions.

1 Introduction

Characterizing causal dependencies between variables is a fundamental problem in science [1, 2, 3]. Such relationships are often described via a directed acyclic graph (DAG) where nodes represent variables and directed edges encode causal links between pairs of variables. One may then consider a

Table 1: Comparison with related work. d denotes the number of features, m denotes the number of learned factors. Because m remains low (e.g., 20), we have $m \ll d$. [†]additive cubic model only.

Related work	non-linear link function	likelihood eval. complexity	DAG penalty eval. complexity	intervention model
NO-TEARS [19]	✗	$O(d^2)$	$O(d^3)$	✗
NO-BEARS [26]	✓ [†]	$O(d^2)$	$O(d^2)$	✗
NO-TEARS-LR [20]	✗	$O(md)$	$O(d^3)$	✗
DCDI [6]	✓	$O(d^2)$	$O(d^3)$	✓
DCD-FG (<i>this work</i>)	✓	$O(md)$	$O(md)$	✓

set of conditional probability distributions in addition to the DAG to define a causal graphical model (CGM) [4]. The graphical model is referred to as “causal” because it provides a clear semantic for defining the effect of interventions on the joint likelihood [5].

The combinatorial nature of the set of DAGs and its size make inference of causal structure from data a hard problem. Indeed, the number of DAGs (or the number of permutations) grows super exponentially in the number of nodes, limiting the practical application of most methods to tens of nodes [6, 7, 8]. This highlights a disparity between the development of the field and emerging data from real-world problems in finance [9, 10], neuroscience [11, 12] and high-throughput biology [13, 14, 15, 16]. For example, experimental advances in biology have enabled the generation of data sets where expression profiles of thousands of RNA transcripts are measured in hundreds of thousands of cells following genetic interventions in each of hundreds or thousands of different genes.

To reduce this computational burden, a promising direction is to limit the complexity of the search space. This idea has become commonplace at the interface of statistics and optimization, where sparsity [17] as well as low-rank assumptions [18] are often exploited in machine learning algorithms. Although sparsity is widely used in causal structure learning [7, 19], the use of low-rank constraints in this specific setting remains largely under-explored, with a few notable exceptions [20, 21]. This may be due to the fact that such an assumption may be hard to incorporate into common methods for DAG learning that rely on graphical constraints or on permutations.

Recently, the NOTEARS methodology [19] introduced a continuous relaxation of DAG learning, effectively closing the gap between causal structure learning and continuous optimization. NOTEARS facilitates incorporating more flexible structural assumptions into DAG learning, such as neural network parametrizations of the conditional probability distributions. Although NOTEARS has been the subject of several follow-up works [22, 23, 24, 25, 26], including learning from interventional data [6], several challenges remain. First, the likelihood function usually decomposes as a product of local likelihoods for each node, and existing options for those local models are either fast to fit but likely underfitting the data (linear models [19]) or are computationally expensive and prone to overfitting (a neural network taking as input all of the other nodes [6]). Second, most methods rely on a differentiable penalty for acyclicity whose evaluation has cubic complexity in the number of nodes. As a result, these methods are impractical for graphs with more than a hundred nodes.

In this work, we investigate both challenges and propose a methodology for large-scale discovery of causal structure and prediction of unseen interventions that scales to millions of samples and thousands of nodes. Our key idea is to limit the search space to what we refer to as factor directed acyclic graphs (f -DAGs), a class of low-rank graphs defined in Section 3.1. This constraint assumes that many nodes share similar sets of parents and children, which is the case in scale-free topologies [20] and many biological systems, where genes act together in programs [3, 27, 28]. Based on this class of graphs, we design a flexible model and a scalable inference procedure (Table 1) that we refer to as Differentiable Causal Discovery of Factor Graphs (DCD-FG).

After introducing the necessary background (Section 2), we define the class of f -DAGs (Section 3) and draw connections to several flavors of matrix factorization. In particular, we show connections between the number of factors in an f -DAG and the Boolean rank [29] of its adjacency matrix. We exploit these connections to present a scalable acyclicity score with linear complexity in the number of observed variables. Finally, we characterize the identifiability of these graphs under an Erdős-Rényi random graph model and prove the instability of the Boolean rank under edge perturbations. The latter analysis highlights that restricting inference to f -DAGs is more efficient in the high-

dimensional causal discovery regime. Then, we posit a flexible class of likelihood models as well as a scalable inference method for our DCD-FG framework (Section 4). Finally, we present runtime experiments, simulation studies, and a case study on single-cell RNA sequencing data with hundreds of genetic interventions (Section 5). In this last challenging instance of interventional data with high-dimensional measurements, we show that our framework outperforms current state-of-the-art causal discovery approaches for predicting the effect of held-out interventions.

2 Background

Our work builds upon continuous relaxations of the causal structure learning problem. We therefore first briefly introduce causal graphical models and then how the inference problem is solved with a gradient-based optimization framework.

2.1 Causal Graphical Models

Following the framework introduced in [5], let $X = (X_1, \dots, X_d)$ denote a set of random variables with a joint probability distribution P . Let $G = (V, E)$ be a DAG where each vertex $v_i \in V$ is associated with a random variable X_i and each edge (v_i, v_j) represents a causal relationship from X_i to X_j . A correspondence between the graph and the probability distribution P is obtained via the factorization condition

$$P(X_1, \dots, X_d) = \prod_{j=1}^d P(X_j | X_{\pi(j)}), \quad (1)$$

where $X_{\pi(j)}$ denotes the vector of random variables formed by all parents of node v_j in G . We refer to a pair (P, G) that satisfies the factorization condition as a causal graphical model (CGM).

Unlike classical graphical models, CGMs provide a principled way to model interventions [30]. With interventional data, each observation is measured under a specific regime k with interventional joint density $P^{(k)}$. For each regime, a subset of the target variables \mathcal{I}_k is subject to intervention. Each of these interventions affects the relationship between the target node and its parents, by altering the conditional distribution. In the case of perfect interventions [8], the dependency of intervened upon nodes from their parents is removed, and the interventional joint density $P^{(k)}$ becomes

$$P^{(k)} = \prod_{j \notin \mathcal{I}_k} P(X_j | X_{\pi(j)}) \prod_{j \in \mathcal{I}_k} P^{(k)}(X_j), \quad (2)$$

where $P^{(k)}$ models the effect of the perfect (stochastic) interventions on each targeted feature of \mathcal{I}_k .

2.2 Differentiable Causal Structure Learning

A significant challenge is to identify and learn CGMs from data when the causal relationships between features are not known beforehand. Several methods have been proposed for this problem, such as constraint-based methods (e.g., the PC algorithm [8]), score-based methods (e.g., GSP [31]), and their extensions for modeling interventions (e.g., IGSP [7]), all reviewed in [32].

The NOTEARS methodology [19] proposes to solve a continuous relaxation of the optimization problem of score-based methods, which in the case of observational data can be written as

$$\min_{\mathbf{W}} \frac{1}{n} \sum_{i=1}^n \|X^i - \mathbf{W}X^i\|_2^2 + \lambda \|\mathbf{W}\|_1 \quad \text{such that} \quad \text{Tr} \exp\{\mathbf{W} \circ \mathbf{W}\} = d, \quad (3)$$

where n denotes the total number of i.i.d. observations, $X^i \in \mathbb{R}^d$ denotes the i -th observation of X , \circ denotes the Hadamard product, $\mathbf{W} \in \mathbb{R}^{d \times d}$ denotes the parameters of a linear Gaussian conditional distribution, assuming equal variance for all nodes, and $\lambda > 0$ denotes a tuning parameter. The search space is restricted to DAGs by enforcing that the trace of the exponential (tr-exp) of $\mathbf{W} \circ \mathbf{W}$ is equal to its dimension d . Importantly, evaluating the tr-exp of $\mathbf{W} \circ \mathbf{W}$ as well its gradient with respect to \mathbf{W} has $O(d^3)$ time complexity, which makes it potentially prohibitive for large-scale applications.

This fundamental work has been subject to multiple extensions, of which the most relevant ones are listed in Table 1. First, different models of relationships between variables were introduced with

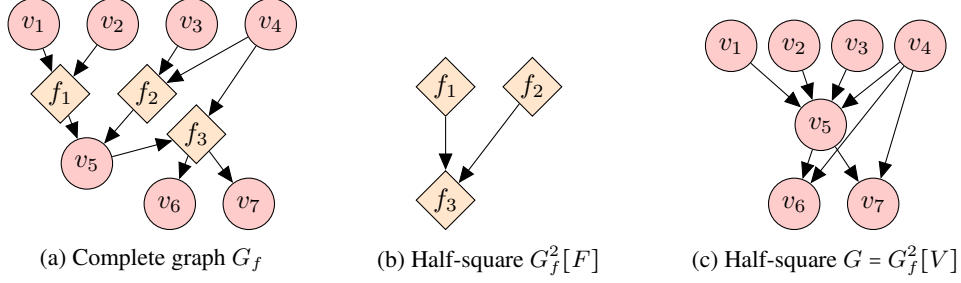


Figure 1: A factor graph and its induced half-square graphs. Red circles represent variable nodes. Orange diamonds represent factor nodes.

the aim of better fitting the data, including several non-linear models, such as neural networks [6, 22, 24, 33, 23]. Because these methods use one neural network per conditional distribution (or one deep sigmoidal flow), they are computationally expensive, as emphasized in [6]. The additive cubic model proposed by NOBEARS [26] does not have these scalability issues, but may be of limited flexibility. To reduce the number of parameters, graph neural networks have been proposed [25], but that architecture cannot be easily applied to the case of interventional data. In addition, NOTEARS-LR [20] proposes a low-rank decomposition of the linear model from NOTEARS but did not consider that the computational complexity could become a bottleneck for large graphs.

Second, studies also investigated variants of the acyclicity penalty. [25] proposes a matrix power variant of the trace exponential criterion, for numerical stability. NOBEARS [26] uses an algebraic characterization of acyclicity based on the spectral radius of the adjacency matrix, that can be approximated in $O(d^2)$. LoRAM [21] exploits a low-rank assumption to obtain a $O(d^2m)$ acyclicity score, where m denotes the rank. However, the proposed framework is tailored to projections of DAG into a low-rank space but not to causal discovery learning.

3 Factor Directed Acyclic Graphs

Next, we introduce factor directed acyclic graphs (f -DAGs) and draw connections to low-rank matrix factorizations. Then, we motivate their use in causal inference by studying the effect of edge perturbation on their rank. Additionally, we provide two differentiable acyclicity penalties computable in linear time in the number of nodes for a fixed set of factors by exploiting the low-rank structure.

3.1 Definitions and relationship to low-rank decomposition

Factor graphs, especially undirected ones, are commonly used in the graphical models literature to factorize probability distributions and describe the complexity of message passing algorithms [34]. In this work, we use them to construct causal graphs over features. In addition to the set of feature vertices $V = \{v_1, \dots, v_d\}$, we consider a set of factor vertices $F = \{f_1, \dots, f_m\}$, for $m \in \mathbb{N}$. When the edge set E links only vertices of different types, the graph $G_f = (V, F, E)$ is a bipartite graph and we refer to it as a factor directed graph (f -DiGraph). If G_f additionally does not contain cycles, we call it an f -DAG. G_f canonically induces two half-square graphs $G_f^2[V]$ and $G_f^2[F]$, defined by drawing an edge between vertices of V (or F) of distance exactly two in G_f (see example in Figure 1). Unless otherwise mentioned, we will refer to $G = G_f^2[V]$ as the half-square of G_f over vertices. We define the set of half-square graphs of f -DiGraphs with d variables and m factors as

$$\mathcal{G}_d^m = \{G = G_f^2[V] \mid G_f = (V, F, E) \text{ is a factor directed graph and } |F| = m\}. \quad (4)$$

Intriguingly, the set \mathcal{G}_d^m may be identified as the set of matrices with Boolean rank [29] of at most m .

Proposition 1 (Bounded Boolean rank of half-square adjacency matrix). *For a factor graph $G_f = (V, F, E)$, let $\mathbf{U} \in \{0, 1\}^{d \times m}$ (resp. $\mathbf{V} \in \{0, 1\}^{m \times d}$) be the binary matrix encoding the presence or absence of edges directed towards factor nodes (resp. variable nodes), according to E . The adjacency matrix $A(G)$ of the half-square graph G may be decomposed as $A(G) = \mathbf{U} \diamond \mathbf{V}$ where \diamond denotes the Boolean matrix product, $(\mathbf{U} \diamond \mathbf{V})_{ij} = \bigvee_{k=1}^m \mathbf{U}_{ik} \wedge \mathbf{V}_{kj}$, $i, j \in [d]$. Consequently, $A(G)$*

has Boolean rank bounded above by m . Conversely, every adjacency matrix over the feature nodes with Boolean rank bounded by m can be written as half-square of an f -DiGraph with m factors.

This result, proven in Appendix A, establishes a connection between inference of causal f -DAGs and Boolean matrix factorization. Additionally, it is easy to notice that the (integer-valued) matrix product UV provides a valid (weighted) adjacency matrix for G . In this work, we show that the Boolean decomposition is suited for theoretical analysis of the method, while the linear one is useful for efficient algorithm design. We further note that this proposed class of graphs is smaller than the one arising from adjacency matrices with (unconstrained) linear matrix rank bounded by m , which we detail further in Appendix A.4.

3.2 Statistical Properties of Random Causal Factor Graphs

An important theoretical question pertains to the assumptions necessary for identification of acyclic graphs in \mathcal{G}_d^m (which we denote by \mathcal{D}_d^m) from data. Under the classical set of assumptions (causal sufficiency, causal Markov property and faithfulness), we may identify the causal DAG from observational data only up to its Markov equivalence class (MEC) [35]. However, graphs in \mathcal{D}_d^m can have many v -structures (emerging from having several feature parents), potentially making them identifiable. Indeed, we prove in Appendix B that under an adapted Erdős-Rényi random graph model [36] over \mathcal{D}_d^m , graphs are identifiable with high probability (i.e., their MEC is reduced to one graph). We also verified this with simulations (Figure 2A).

Although valid, the previous result may be disconnected from real-world applications in high-dimensional regimes for which stronger assumptions are required (e.g., strong faithfulness [37]), but rarely hold [38]. More concretely, we expect errors in the estimated skeleton of the feature node graph. As a toy model of these errors, we assume the true causal graph G is in \mathcal{G}_d^m and apply a stochastic edge perturbation operator Λ that randomly removes or adds one edge to G . While there are no general rules as to how identifiability is changed under these perturbations [39] (i.e., the size of the MEC could increase or decrease), we show that the Boolean rank of the graph strictly increases with high probability:

Theorem 1 (Boolean rank instability for edge perturbation). *Let $G \in \mathcal{G}_d^m$ be sampled according to an Erdős-Rényi random directed graph model. The probability that adding or removing an edge increases the Boolean rank is arbitrarily high for large d :*

$$\mathbb{P}(\text{Rank}_{\mathcal{B}}(\Lambda(G)) > \text{Rank}_{\mathcal{B}}(G)) \geq 1 - \alpha q^d, \quad (5)$$

where $\text{Rank}_{\mathcal{B}}$ denotes the Boolean rank, and $\alpha > 0$ and $q \in (0, 1)$ depend on m and the parameters of the random graph model.

Precise definitions of the random graph model and proof appear in Appendix C. This result, analogous to the upper semicontinuity of the matrix rank, suggests that in noisy settings, the skeleton of graphs in \mathcal{D}_d^m may be more easily recoverable compared to arbitrary DAGs. We verified those results with simulations (Figure 2B) for small graphs using a mixed integer linear programming approach [40]. We performed a larger-scale analysis by randomly perturbing a fraction q of the edges in the graph and reporting the resulting matrix rank¹ of the adjacency matrix for larger graphs (Figure 2C).

3.3 Characterizing Acyclicity of Factor Graphs

We start by relating the acyclicity of a f -DiGraph with the one of its induced half-squares. A simple graphical argument is enough to show that acyclicity for a f -DiGraph need only be enforced on the smaller of its half-square graphs.

Lemma 1 (Induced acyclicity). *Let $G = (V, F, E)$ be an f -DiGraph. Then,*

$$G_f \text{ is acyclic} \Leftrightarrow G = G_f^2[V] \text{ is acyclic} \Leftrightarrow G_f^2[F] \text{ is acyclic.} \quad (6)$$

The proof can be found in Appendix D. We further note that the matrix UV (VU , resp.) counts the number of paths between two nodes in V (F , resp.) and is thus a valid (weighted) adjacency matrix

¹Using the matrix rank is only a heuristic approximation of the quantitative increase in complexity of the underlying matrix, because in general it provides neither an upper nor a lower bound on the Boolean rank [41].

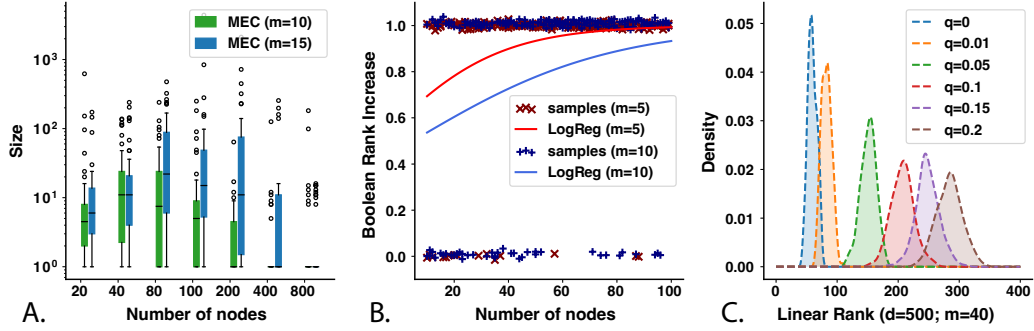


Figure 2: Properties of simulated Erdős-Rényi random f -DiGraphs. (A) Size of MEC of the simulated half-square graph with varying m and d . (B) Probability of increase of Boolean rank after edge perturbation (Theorem 1). A single point denotes the result of an experiment, the solid line is the probability estimated by logistic regression. (C) Matrix rank change after multiple random edge perturbations.

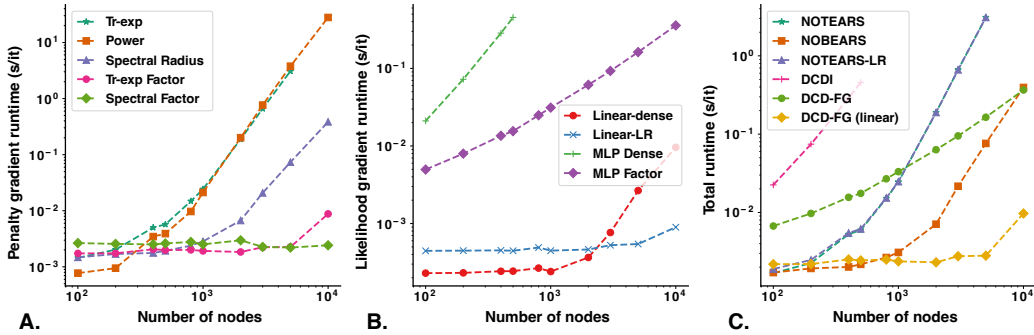


Figure 3: Runtime analysis. Time for gradient calculation of likelihood (A), penalty (B) or their sum (C) for different variants of optimization-based DAG inference method (on one NVIDIA Tesla T4 GPU with 15Gb of RAM). We selected a batch size of 128 datapoints and a number of $m = 40$ factors for all experiments. If a value is non-reported, a memory error was raised at runtime. NOTEARS and NOTEARS-LR have almost identical runtime in this analysis.

for G ($G_f^2[F]$, resp.). As a result, we may characterize acyclicity by applying the tr-exp penalty to the matrix $\mathbf{V}\mathbf{U}$ in time $O(m^3 + m^2d)$ compared to the $O(d^3 + md^2)$ steps needed for evaluating the penalty on $\mathbf{U}\mathbf{V}$. Alternatively, we may use the spectral radius of the adjacency matrix as an acyclicity score [26] that can be approximately computed in $O(Tmd)$ steps, with T iterations of the power method between each gradient step (details in Appendix D). The resulting computational gains are showcased in Figure 3A. For small m , both variants have a similar runtime.

4 Differentiable Discovery of Causal Factor Graphs

To define a CGM, we couple the f -DiGraph with a likelihood model. We follow recent work that partitions the parameter space into conditional distribution parameters Θ , and parameters Φ encoding the causal graph [6]. In particular, let us assume we have at our disposal a parameterized distribution $\mathbf{M}(\Phi) = [\mathbf{U}(\Phi), \mathbf{V}(\Phi)]$ over adjacency matrices of f -DiGraphs. The score function, assuming perfect interventions, is defined as:

$$\mathcal{S}(\Phi, \Theta) = \mathbb{E}_{\mathbf{M}' \sim \mathbf{M}(\Phi)} \left[\sum_{k=1}^K \mathbb{E}_{X \sim P_{\text{data}}^{(k)}} \sum_{j \notin \mathcal{I}_k} \log p_{\Theta}^j(X_j; \mathbf{M}'_j, X_{-j}) \right] - \lambda \|\mathbb{E}[\mathbf{M}(\Phi)]\|_1, \quad (7)$$

where $P_{\text{data}}^{(k)}$ denotes the distribution of data points X under regime k , p_{Θ}^j denotes a density model for feature X_j , conditioned on all other features X_{-j} that are parents of the feature j according to the

sampled matrix \mathbf{M}'_j . We optimize the score function \mathcal{S} under an acyclicity constraint,

$$\max_{\Phi, \Theta} \mathcal{S}(\Phi, \Theta) \text{ such that } \mathcal{C}(\mathbb{E}[\mathbf{M}(\Phi)]) = 0, \quad (8)$$

where \mathcal{C} may correspond to either the spectral radius, or the tr-exp characterization of acyclicity. Numerically, first-order optimization techniques with reparameterized gradients and the augmented Lagrangian method are used to solve problem (8). We outline here some key features of DCD-FG, and provide the complete implementation details in Appendix E.

Differentiable Sampling of Factor Graphs A first important challenge specific to our work is constructing a density $\mathbf{M}(\Phi)$ over f -DiGraphs. The DCDI framework [6], and a few earlier methods [23, 42], parameterize the set of adjacency matrices with entry-wise Gumbel-sigmoid [43] samples, and zeros in the diagonal entries. Naively applying this parameterization for sampling matrices $\mathbf{M} = [\mathbf{U}, \mathbf{V}]$ causes the induced feature graphs to have a large number of self-loops, i.e., edges of the form (v, v) that we found to be detrimental to the performance of the model. To circumvent this issue, we propose an alternative model in which the matrices \mathbf{U} and \mathbf{V} are correlated. More precisely, for $\mathbf{W} \in \{0, -1, 1\}^{d \times m}$ sampled according to a Gumbel-softmax distribution [43], the entries of \mathbf{U} and \mathbf{V} are constructed from \mathbf{W} as $\mathbf{U}_{ij} = \mathbb{1}\{\mathbf{W}_{ij} = 1\}$ and $\mathbf{V}_{ji} = \mathbb{1}\{\mathbf{W}_{ij} = -1\}$ for $i \in [d], j \in [m]$. Because the entries \mathbf{U}_{ij} and \mathbf{V}_{ji} may never be both equal to 1, there are no self-loops in the induced half-square graph.

A hybrid likelihood model A second important challenge is to propose flexible density models p_{Θ} that have reasonable runtime as well as enough capacity for practical purposes. For this, we further exploit the semantics of the factor graph by introducing deterministic factor variables h_f at each factor node $f \in F$. These variables are calculated as the output of a multi-layer perceptron on the input variables of each factor defined by the matrix \mathbf{U} , $h_f = \text{MLP}(\mathbf{U}_{:,f} \circ X; \Theta_f)$, for neural networks parameters Θ_f . Then, the conditional distribution of each node depends linearly on its parent factors defined by the matrix \mathbf{V} , $X_j \sim \text{Normal}(\alpha_j^{\top}(\mathbf{V}_{:,j} \circ h) + \beta_j, \sigma_j^2)$ for parameters $\alpha_j \in \mathbb{R}^m$, $\beta_j \in \mathbb{R}$, $\sigma_j > 0$. The resulting computational gains are highlighted in Figure 3B,C. Although we present here the specific case of a Gaussian likelihood model, the same strategy may be adopted for more complex distributional models such as sigmoidal flows [6].

5 Experiments

We tested DCD-FG on both synthetic and real-world data sets with $d = 100$ to $d = 1,000$, and a large number of observations ($n \geq 50,000$). In this large-scale setting, many state-of-the-art causal discovery methods fail to terminate (DCDI and IGSP). Therefore, we compared DCD-FG to NOTEARS [19], its additive non-linear variant NOBEARS [26] and its linear low-rank variant NOTEARS-LR [20]. In order to have a baseline that is external to the NOTEARS framework, we applied IGSP (after feature aggregation via clustering with different resolutions when necessary for a reasonable runtime). For every model, we performed a hyperparameter search using a goodness of fit metric on a small validation set. We provide further details on all experiments, including the grids used for hyperparameter search, as well as supplementary experiments, in Appendix F.

5.1 Gaussian Structural Causal Models

We consider synthetic data sets with perfect interventions and known targets. Each data set has $d = 100$ nodes and $n = 50,000$ observations, sampled from interventional distributions governed by either a linear causal mechanism [44] or a nonlinear causal mechanism with additive noise (NN) [45]. Graphs are sampled from an Erdős-Rényi random directed graph model with $m = 10$ factors. A total of $K = 100$ interventions were performed, each sampling up to 3 target nodes. Datapoints from 20 interventional regimes were held-out for model evaluation.

We assessed the performance of each method by the negative log-likelihood of datapoints from unseen interventions (Interventional NLL) [46], as well as two metrics comparing the estimated graph to the ground truth graphs: the structural Hamming distance (SHD), and the precision and recall of edge detection. We report results for 10 randomly generated graphs and data sets in Figure 4. NOTEARS-LR and DCD-FG both outperformed all methods for all metrics on the linear dataset ($p < 0.01$, Wilcoxon signed-rank test), showing that both effectively exploit the low-rank structure

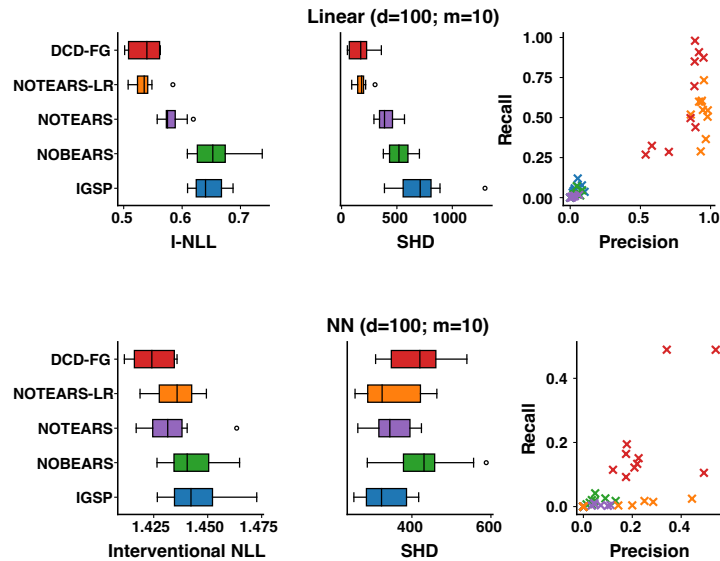


Figure 4: Results on simulated Gaussian structural causal models (Section 5.1).

of the causal graph. On the non-linear (NN) dataset, DCD-FG outperformed all methods in terms of interventional NLL, as well as recall and F1-score (combining precision and recall, Appendix F) ($p < 0.01$, Wilcoxon signed-rank test). DCD-FG has high SHD but we attribute this to the fact that all methods besides DCD-FG discover very sparse graphs.

5.2 Genetic Interventions and Gene Expression Data

As an application to real world data, we present an experiment focused on causal learning of gene regulatory networks from gene expression data with genetic interventions, a central problem in modern molecular biology [3, 47, 48]. Although this particular task has been studied by computational biologists for over two decades, there have been substantial experimental advances in the last few years. In particular, a method called Perturb-Seq now allows us to perform interventions targeting hundreds or thousands of genes and measure the effect on full gene expression profiles in hundreds of thousands of single cells using single cell RNA-seq [13]. Surprisingly, however, little to no causal learning work has focused on these advanced datasets. A few notable exceptions, such as [35], focused on early data for which the benchmarked methods were tractable ($d = 24$ genes).

We focus on a recent Perturb-CITE-seq experiment [14] that contains expression profiles from 218,331 melanoma (cancer) cells, after interventions targeting each of 249 genes. Each measurement from a single-cell combines the identity of the intervention (target gene) and a count vector where each entry is the expression level of each gene in the genome. Because of experimental limitations [49], we observe signal only for a subset of several thousand genes (here we selected $d = 1,000$ genes) out of the approximately 20,000 genes in the genome. This dataset includes patient-derived melanoma cells with same genetic interventions but exposed to three conditions: co-culture with T cells derived from the patient’s tumor (73,114 cells) (which can recognize and kill melanoma cells), interferon (IFN)- γ treatment (87,590 cells) and control (57,627 cells) that we treat as three separate datasets. The goal of the experiment was to identify gene networks in the melanoma cancer cells that either confer resistance or sensitivity to T cell mediated killing, to identify targets for therapeutic intervention in cancer. For every dataset, we retain cells from 20% of the interventions as a test set unavailable during training.

We applied our baseline methods as well as DCD-FG to each of the three datasets. Because we do not have a ground truth causal graph, we use datapoints from held-out interventions to evaluate the models [46], reporting both the interventional NLL (I-NLL) and the mean absolute error (I-MAE) across those interventions (Figure 5). Note that accurately predicting the outcome of genetic interventions that were not measured experimentally is of high utility to biologists.

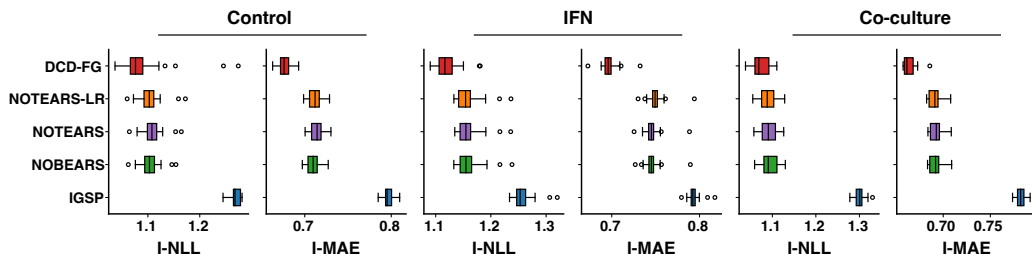


Figure 5: Results on the Perturb-CITE-seq dataset [14] (Section 5.2, lower is better).

DCD-FG outperformed all variants of the NOTEARS method by a large margin, including NOTEARS-LR, and for all metrics ($p < 0.01$, Wilcoxon signed-rank test). In order to diagnose the poor performance of the competing methods, we looked at the number of inferred edges by each method. All variants of NOTEARS identified extremely sparse graphs (less than a hundred edges for NOTEARS and NOBEARS, and a few thousand edges for NOTEARS-LR), which may explain their inability to predict the effect of held-out interventions. Interestingly, IGSP identified hundreds of thousands of edges, a number that was comparable to DCD-FG, but still had poor performance. This suggests that the IGSP-inferred graph did not recapitulate well the causal relationships between genes.

In particular, we carefully examined the f -DAG G_f obtained with the best performing model from our hyperparameter sweep on the IFN- γ treated cells. That model has $m = 20$ factors, and the half-square $G_f^2[V]$ has 196,303 edges. On average, each module has 194 ingoing edges and 116 outgoing edges. To facilitate visualization, we display the half-square over factors $G_f^2[F]$ in Figure 6.

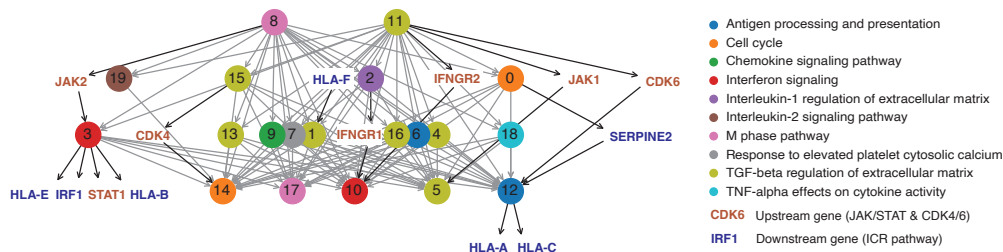


Figure 6: Half-square $G_f^2[F]$ (completed with a few genes) of an f -DAG identified by DCD-FG on IFN- γ treated malignant cells with interventions. Circles: factors, colored by the gene set enrichment analysis result for its incoming and outgoing genes. Empty nodes: genes, labelled name. Red/blue: genes expected to be up or downstream (resp.) by prior biological knowledge.

To begin to assess the biological relevance of the graph, we performed two analyses. First, we tested the list of incoming and outgoing genes for each factor for enrichment in genes from known biological processes (via [50]). The top hits (node colors in Figure 6) captured many relevant processes in perturbed malignant cells treated by IFN including antigen presentation (needed for recognition by the T cells), multiple innate immune and related signaling pathways (chemokine, interferon, TNF- α , and TGF- β signaling; all can affect the ability of immune cells to target cancer cells) and stages of the cell cycle. Thus, the graph captured key regulated processes in the response. Second, and more crucially, to highlight key genes in the context of the graph, we displayed them onto the half-square $G_f^2[F]$ based on their strongest link (details in Appendix F). As a proof of concept, we focused on two classes of genes: key known regulators we expect to be positioned upstream, such as the interferon receptors (IFNGR1 and 2) which sense the IFN signal, JAK/STAT, needed to transduce the signal, and CDK4 and 6, which regulate the cell cycle but also repress antigen presentation genes; and others we expect to be downstream, in particular those from an immune cancer resistance pathway we previously discovered in patient tumors (ICR [51]; downstream) in Figure 6. Excitingly, while no such information was used to constrain the model, it captured these ordered relations, including a causal path from the interferon receptors to interferon signaling modules, from JAK to interferon signaling to STAT, IRF1 and HLA genes, from CDK4 to the cell cycle, and from CDK6 and the IFNGR1 to HLA genes (antigen presentation, MHC I genes) ([14, 51] and references therein). Notably,

there are also some connections that may not be borne out biologically, such as the separation of CDK4 / CDK6 to different pathways. Overall, DCD-FG is a promising starting point for deciphering gene regulation at the scale of the whole transcriptome with Perturb-seq data, and predicting the outcome of interventions that were not tested experimentally.

6 Discussion

We have proposed DCD-FG, a novel approach for large-scale causal discovery that restricts the search space to factor directed acyclic graphs, and efficiently exploits this structure during inference. Our theoretical results suggest that this class of graphs offers statistical benefits under either the faithfulness assumption or under some stochastic edge perturbation model in random graphs. Our numerical experiments show that in important real-world examples, our method outperforms NOTEARS, NOBEARS as well as low-rank variants of those methods.

Since the publication of NOTEARS [19], two manuscripts highlighted that the method’s evaluation may be confounded by the design of the simulations [52, 53]. However, those studies exclusively focus on causal discovery from observational data. The recent results obtained by DCDI on interventional data with a more suitable simulation design [6], as well as the results of this manuscript on real data show the potential promise of the overall framework.

Recently, several other papers identified the acyclicity constraint as a bottleneck for causal discovery learning, and propose to either use the constraint as a soft penalty [54], or discard it from the objective function [55] by using a different parameterization of the causal graph learning approach, and interventional data. Although the approach from [54] is currently restricted to learning linear causal models from observational data, [55] could complement our approach by simplifying the optimization procedure but still explicitly model low-rank interactions.

We presented an application of DCD-FG to a large-scale high-throughput gene expression dataset with genetic perturbations ("Perturb-Seq"). The method had better predictive performance for held-out perturbations than state-of-the-art, and identified both well established relations and new intriguing ones, offering great utility to biologists. Notably, some of the causal relationships may not be accurate, and it is likely that several assumptions of the underlying model may be violated. The biological evaluation and validation of the method will therefore be important to more deeply assess the performance of DCD-FG.

Future work will explore the specification of the noise model, for which count distributions (potentially as part of a latent variable model) may be more appropriate [56], as well as the absence of confounding variables such as cell cycle [14]. Additionally, we plan to investigate extending the framework of DCD-FG to the inference of causal models with feedback loops [57] in order to generate an even more exact and biologically interpretable causal graph. Finally, having a Bayesian alternative of DCD-FG (e.g., based on [58]) would allow scientists to apply those methods for automated experimental design and scientific discovery.

Acknowledgments and Disclosure of Funding

We thank Sébastien Lachapelle, Philippe Brouillard, Alexandre Drouin, Chandler Squires and Gonçalo Rui Alves Faria for insightful conversations about causal structure learning problems. We thank Natasa Tagasovska, Stephen Ra, and Kyunghyun Cho for general conversations about causal inference and biology. We also acknowledge Katie Geiger-Schuller, Chris Frangieh, Taka Kudo, Josh Weinstock and Basak Eraslan for discussions about Perturb-seq and the Perturb-CITE-seq dataset. We warmly thank Geoffrey Négiar, Natasa Tagasovska, and Tara Chari for their constructive criticisms on draft of this paper.

Disclosures: Romain Lopez and Jan-Christian Huetter are employees of Genentech. Jan-Christian Huetter has equity in Roche. Jonathan Pritchard acknowledges support from grant R01HG008140 from the National Human Genome Research Institute. Aviv Regev is a co-founder and equity holder of Celsius Therapeutics and an equity holder in Immunitas. She was an SAB member of ThermoFisher Scientific, Syros Pharmaceuticals, Neogene Therapeutics, and Asimov until July 31st, 2020; she has been an employee of Genentech since August 1st, 2020, and has equity in Roche.

References

- [1] Karen Sachs, Omar Perez, Dana Pe’er, Douglas A Lauffenburger, and Garry P Nolan. Causal protein-signaling networks derived from multiparameter single-cell data. *Science*, 308(5721):523–529, 2005.
- [2] Bin Zhang, Chris Gaiteri, Liviu-Gabriel Bodea, Zhi Wang, Joshua McElwee, Alexei A Podtelezchnikov, Chunsheng Zhang, Tao Xie, Linh Tran, Radu Dobrin, et al. Integrated systems approach identifies genetic nodes and networks in late-onset alzheimer’s disease. *Cell*, 153(3):707–720, 2013.
- [3] Eran Segal, Dana Pe’er, Aviv Regev, Daphne Koller, and Nir Friedman. Learning module networks. *Journal of Machine Learning Research*, 6(4), 2005.
- [4] Daphne Koller and Nir Friedman. *Probabilistic Graphical Models*. MIT Press, 2009.
- [5] Jonas Peters, Dominik Janzing, and Bernhard Schölkopf. *Elements of Causal Inference - Foundations and Learning Algorithms*. MIT Press, 2017.
- [6] Philippe Brouillard, Sébastien Lachapelle, Alexandre Lacoste, Simon Lacoste-Julien, and Alexandre Drouin. Differentiable causal discovery from interventional data. In *Advances in Neural Information Processing Systems*, 2020.
- [7] Yuhao Wang, Liam Solus, Karren Dai Yang, and Caroline Uhler. Permutation-based causal inference algorithms with interventions. In *Advances in Neural Information Processing Systems*, 2017.
- [8] Peter Spirtes, Clark N. Glymour, and Richard Scheines. *Causation, Prediction, and Search*. The MIT Press, 2000.
- [9] Theo Diamandis, Yonathan Murin, and Andrea Goldsmith. Ranking causal influence of financial markets via directed information graphs. In *Annual Conference on Information Sciences and Systems (CISS)*, 2018.
- [10] Katerina Rigana, Ernst C Wit, and Samantha Cook. Using network-based causal inference to detect the sources of contagion in the currency market. *arXiv*, 2021.
- [11] Rakesh Malladi, Giridhar Kalamangalam, Nitin Tandon, and Behnaam Aazhang. Identifying seizure onset zone from the causal connectivity inferred using directed information. *IEEE Journal of Selected Topics in Signal Processing*, 10(7):1267–1283, 2016.
- [12] Joseph Ramsey, Madelyn Glymour, Ruben Sanchez-Romero, and Clark Glymour. A million variables and more: the fast greedy equivalence search algorithm for learning high-dimensional graphical causal models, with an application to functional magnetic resonance images. *International Journal of Data Science and Analytics*, 3(2):121–129, 2017.
- [13] Atray Dixit, Oren Parnas, Biyu Li, Jenny Chen, Charles P Fulco, Livnat Jerby-Arnon, Nemanja D Marjanovic, Danielle Dionne, Tyler Burks, Raktima Raychowdhury, et al. Perturb-seq: dissecting molecular circuits with scalable single-cell RNA profiling of pooled genetic screens. *Cell*, 167(7):1853–1866, 2016.
- [14] Chris J Frangieh, Johannes C Melms, Pratiksha I Thakore, Kathryn R Geiger-Schuller, Patricia Ho, Adrienne M Luoma, Brian Cleary, Livnat Jerby-Arnon, Shruti Malu, Michael S Cuomo, et al. Multimodal pooled Perturb-CITE-seq screens in patient models define mechanisms of cancer immune evasion. *Nature Genetics*, 53(3):332–341, 2021.
- [15] Thomas M Norman, Max A Horlbeck, Joseph M Replogle, Alex Y Ge, Albert Xu, Marco Jost, Luke A Gilbert, and Jonathan S Weissman. Exploring genetic interaction manifolds constructed from rich single-cell phenotypes. *Science*, 365(6455):786–793, 2019.
- [16] Joseph M. Replogle, Reuben A. Saunders, Angela N. Pogson, Jeffrey A. Hussmann, Alexander Lenail, Alina Guna, Lauren Mascibroda, Eric J. Wagner, Karen Adelman, Jessica L. Bonnar, Marco Jost, Thomas M. Norman, and Jonathan S. Weissman. Mapping information-rich genotype-phenotype landscapes with genome-scale Perturb-seq. *Cell*, 2022.
- [17] Trevor Hastie, Robert Tibshirani, and Martin Wainwright. *Statistical Learning with Sparsity: The Lasso and Generalizations*. Chapman & Hall/CRC, 2015.
- [18] Yehuda Koren, Robert Bell, and Chris Volinsky. Matrix factorization techniques for recommender systems. *Computer*, 42(8):30–37, 2009.
- [19] Xun Zheng, Bryon Aragam, Pradeep Ravikumar, and Eric P. Xing. DAGs with NO TEARS: continuous optimization for structure learning. In *Advances in Neural Information Processing Systems*, 2018.
- [20] Zhuangyan Fang, Shengyu Zhu, Jiji Zhang, Yue Liu, Zhitang Chen, and Yangbo He. Low rank directed acyclic graphs and causal structure learning. *arXiv*, 2020.
- [21] Shuyu Dong and Michèle Sebag. From graphs to DAGs: a low-complexity model and a scalable algorithm. *arXiv*, 2022.
- [22] Sébastien Lachapelle, Philippe Brouillard, Tristan Deleu, and Simon Lacoste-Julien. Gradient-based neural DAG learning. In *International Conference on Learning Representations*, 2020.

- [23] Ignavier Ng, Shengyu Zhu, Zhuangyan Fang, Haoyang Li, Zhitang Chen, and Jun Wang. Masked gradient-based causal structure learning. In *SIAM International Conference on Data Mining (SDM)*, 2022.
- [24] Xun Zheng, Chen Dan, Bryon Aragam, Pradeep Ravikumar, and Eric P. Xing. Learning sparse nonparametric DAGs. In *International Conference on Artificial Intelligence and Statistics*, 2020.
- [25] Yue Yu, Jie Chen, Tian Gao, and Mo Yu. DAG-GNN: DAG structure learning with graph neural networks. In *International Conference on Machine Learning*, 2019.
- [26] Hao-Chih Lee, Matteo Danieletto, Riccardo Miotto, Sarah T. Cherng, and Joel T. Dudley. Scaling structural learning with NO-BEARS to infer causal transcriptome networks. In *Pacific Symposium on Biocomputing*, 2019.
- [27] Brian Cleary, Le Cong, Anthea Cheung, Eric S Lander, and Aviv Regev. Efficient generation of transcriptomic profiles by random composite measurements. *Cell*, 171(6):1424–1436, 2017.
- [28] Graham Heimberg, Rajat Bhatnagar, Hana El-Samad, and Matt Thomson. Low dimensionality in gene expression data enables the accurate extraction of transcriptional programs from shallow sequencing. *Cell Systems*, 2(4):239–250, 2016.
- [29] Pauli Miettinen and Stefan Neumann. Recent developments in Boolean matrix factorization. In *International Joint Conferences on Artificial Intelligence*, 2021.
- [30] Frederick Eberhardt and Richard Scheines. Interventions and causal inference. *Philosophy of Science*, 2007.
- [31] Liam Solus, Yuhao Wang, and Caroline Uhler. Consistency guarantees for greedy permutation-based causal inference algorithms. *arXiv*, 2017.
- [32] Clark Glymour, Kun Zhang, and Peter Spirtes. Review of causal discovery methods based on graphical models. *Frontiers in Genetics*, 10:524, 2019.
- [33] Joris M Mooij, Sara Magliacane, and Tom Claassen. Joint causal inference from multiple contexts. *Journal of Machine Learning Research*, 2020.
- [34] Hans-Andrea Loeliger. An introduction to factor graphs. *IEEE Signal Processing Magazine*, 21(1):28–41, 2004.
- [35] Karren D. Yang, Abigail Katcoff, and Caroline Uhler. Characterizing and learning equivalence classes of causal DAGs under interventions. In *International Conference on Machine Learning*, 2018.
- [36] Paul Erdős, Alfréd Rényi, et al. On the evolution of random graphs. *Publication of the Mathematical Institute of the Hungarian Academy of Sciences*, 5(1):17–60, 1960.
- [37] Samuel Wang and Mathias Drton. High-dimensional causal discovery under non-Gaussianity. *Biometrika*, 107(1):41–59, 10 2019.
- [38] Caroline Uhler, Garvesh Raskutti, Peter Bühlmann, and Bin Yu. Geometry of the faithfulness assumption in causal inference. *The Annals of Statistics*, pages 436–463, 2013.
- [39] Marco F Eigenmann, Preetam Nandy, and Marloes H Maathuis. Structure learning of linear gaussian structural equation models with weak edges. In *Uncertainty in Artificial Intelligence (UAI)*, 2017.
- [40] Reka A Kovacs, Oktay Gunluk, and Raphael A Hauser. Binary matrix factorisation via column generation. In *AAAI Conference on Artificial Intelligence*, volume 35, pages 3823–3831, 2021.
- [41] Derek DeSantis, Erik Skau, Duc P. Truong, and Boian Alexandrov. Factorization of binary matrices: Rank relations, uniqueness and model selection of boolean decomposition. *ACM Transactions on Knowledge Discovery Data*, 2022.
- [42] Diviyani Kalainathan, Olivier Goudet, Isabelle Guyon, David Lopez-Paz, and Michèle Sebag. Structural agnostic modeling: Adversarial learning of causal graphs. *arXiv*, 2018.
- [43] Chris J. Maddison, Andriy Mnih, and Yee Whye Teh. The concrete distribution: A continuous relaxation of discrete random variables. In *International Conference on Machine Learning*, 2017.
- [44] Chandler Squires, Yuhao Wang, and Caroline Uhler. Permutation-based causal structure learning with unknown intervention targets. *Uncertainty in Artificial Intelligence*, 2020.
- [45] Diviyani Kalainathan and Olivier Goudet. Causal discovery toolbox: Uncover causal relationships in python. *Journal of Machine Learning Research*, 21:1–5, 2020.
- [46] Amanda Gentzel, Dan Garant, and David Jensen. The case for evaluating causal models using interventional measures and empirical data. In *Advances in Neural Information Processing Systems*, pages 11722–11732, 2019.
- [47] Nir Friedman, Michal Linial, Iftach Nachman, and Dana Pe’er. Using Bayesian networks to analyze expression data. *Journal of Computational Biology*, 7(3-4):601–620, 2000.

- [48] Dana Pe'er, Aviv Regev, Gal Elidan, and Nir Friedman. Inferring subnetworks from perturbed expression profiles. *Bioinformatics*, 17, 2001.
- [49] Dominic Grun, Lennart Kester, and Alexander van Oudenaarden. Validation of noise models for single-cell transcriptomics. *Nature Methods*, 2014.
- [50] Edward Y Chen, Christopher M Tan, Yan Kou, Qiaonan Duan, Zichen Wang, Gabriela Vaz Meirelles, Neil R Clark, and Avi Ma'ayan. Enrichr: interactive and collaborative HTML5 gene list enrichment analysis tool. *BMC Bioinformatics*, 14(1):1–14, 2013.
- [51] Livnat Jerby-Arnon, Parin Shah, Michael S Cuoco, Christopher Rodman, Mei-Ju Su, Johannes C Melms, Rachel Leeson, Abhay Kanodia, Shaolin Mei, Jia-Ren Lin, et al. A cancer cell program promotes t cell exclusion and resistance to checkpoint blockade. *Cell*, 175(4):984–997, 2018.
- [52] Marcus Kaiser and Maksim Sipos. Unsuitability of NOTEARS for causal graph discovery. *arXiv*, 2021.
- [53] Alexander G. Reisach, Christof Seiler, and Sebastian Weichwald. Beware of the simulated DAG! causal discovery benchmarks may be easy to game. In *Advances in Neural Information Processing Systems*, 2021.
- [54] Ignavier Ng, AmirEmad Ghassami, and Kun Zhang. On the role of sparsity and dag constraints for learning linear dags. In *Advances in Neural Information Processing Systems*, 2020.
- [55] Phillip Lippe, Taco Cohen, and Efstratios Gavves. Efficient neural causal discovery without acyclicity constraints. In *International Conference on Learning Representations*, 2022.
- [56] Romain Lopez, Jeffrey Regier, Michael B Cole, Michael I Jordan, and Nir Yosef. Deep generative modeling for single-cell transcriptomics. *Nature Methods*, 15(12):1053–1058, 2018.
- [57] Jacob W Freimer, Oren Shaked, Sahin Naqvi, Nasa Sinnott-Armstrong, Arwa Kathiria, Christian M Garrido, Amy F Chen, Jessica T Cortez, William J Greenleaf, Jonathan K Pritchard, et al. Systematic discovery and perturbation of regulatory genes in human T cells reveals the architecture of immune networks. *Nature Genetics*, 54(8):1133–1144, 2022.
- [58] Lars Lorch, Jonas Rothfuss, Bernhard Schölkopf, and Andreas Krause. DiBS: Differentiable bayesian structure learning. *Advances in Neural Information Processing Systems*, 34, 2021.
- [59] Tom S. Verma and Judea Pearl. Equivalence and synthesis of causal models. In *Uncertainty in Artificial Intelligence*, 1990.
- [60] Pauli Miettinen, Taneli Mielikäinen, Aristides Gionis, Gautam Das, and Heikki Mannila. The discrete basis problem. *IEEE transactions on knowledge and data engineering*, 20(10):1348–1362, 2008.
- [61] Eric Jang, Shixiang Gu, and Ben Poole. Categorical reparametrization with Gumbel-Softmax. In *International Conference on Learning Representations*, 2017.
- [62] Fabian Pedregosa, Gaël Varoquaux, Alexandre Gramfort, Vincent Michel, Bertrand Thirion, Olivier Grisel, Mathieu Blondel, Andreas Müller, Joel Nothman, Gilles Louppe, Peter Prettenhofer, Ron Weiss, Vincent Dubourg, Jake Vanderplas, Alexandre Passos, David Cournapeau, Matthieu Brucher, Matthieu Perrot, and Édouard Duchesnay. Scikit-learn: Machine learning in Python. *Journal of Machine Learning Research*, 12:2825–2830, 2011.
- [63] Alexander Wolf, Philipp Angerer, and Fabian J Theis. SCANPY: large-scale single-cell gene expression data analysis. *Genome Biology*, 19(1):1–5, 2018.
- [64] Xavier Glorot and Yoshua Bengio. Understanding the difficulty of training deep feedforward neural networks. In *International Conference on Artificial Intelligence and Statistics*, 2010.
- [65] Tijmen Tieleman and Geoffrey Hinton. Lecture 6.5-RMSProp: Divide the gradient by a running average of its recent magnitude. *Coursera: Neural networks for machine learning*, 2012.

Checklist

1. For all authors...
 - (a) Do the main claims made in the abstract and introduction accurately reflect the paper's contributions and scope? [Yes]
 - (b) Did you describe the limitations of your work? [Yes] (Discussion section)
 - (c) Did you discuss any potential negative societal impacts of your work? [Yes] (Discussion section)
 - (d) Have you read the ethics review guidelines and ensured that your paper conforms to them? [Yes]
2. If you are including theoretical results...
 - (a) Did you state the full set of assumptions of all theoretical results? [Yes] (Appendix)
 - (b) Did you include complete proofs of all theoretical results? [Yes] (Appendix)
3. If you ran experiments...
 - (a) Did you include the code, data, and instructions needed to reproduce the main experimental results (either in the supplemental material or as a URL)? [Yes] (Appendix)
 - (b) Did you specify all the training details (e.g., data splits, hyperparameters, how they were chosen)? [Yes] (Appendix)
 - (c) Did you report error bars (e.g., with respect to the random seed after running experiments multiple times)? [Yes] (Box plots in main figure)
 - (d) Did you include the total amount of compute and the type of resources used (e.g., type of GPUs, internal cluster, or cloud provider)? [Yes] (Appendix)
4. If you are using existing assets (e.g., code, data, models) or curating/releasing new assets...
 - (a) If your work uses existing assets, did you cite the creators? [Yes] (Appendix)
 - (b) Did you mention the license of the assets? [Yes] (Appendix)
 - (c) Did you include any new assets either in the supplemental material or as a URL? [Yes] (Appendix)
 - (d) Did you discuss whether and how consent was obtained from people whose data you're using/curating? [N/A]
 - (e) Did you discuss whether the data you are using/curating contains personally identifiable information or offensive content? [N/A]
5. If you used crowdsourcing or conducted research with human subjects...
 - (a) Did you include the full text of instructions given to participants and screenshots, if applicable? [N/A]
 - (b) Did you describe any potential participant risks, with links to Institutional Review Board (IRB) approvals, if applicable? [N/A]
 - (c) Did you include the estimated hourly wage paid to participants and the total amount spent on participant compensation? [N/A]

Appendices

In Appendix A, we present definitions for f -DiGraphs and f -DAGs, as well as general properties of these graphs. In particular, we describe the relationship between adjacency matrices of these graphs and low-rank matrices. In Appendix B, we discuss the concept of identifiability of f -DAGs and Markov Equivalence Classes (MEC). In particular, we show that for a set of fixed factors F and a growing number of variable nodes, random f -DAGs can be identified from observational data. In Appendix C, we prove our main theoretical result on Boolean-rank instability under edge perturbation. In Appendix D, we discuss the time complexity of calculating differentiable acyclicity scores in the case of f -DAGs. In Appendix E, we present the implementation details for DCD-FG. In Appendix F, we provide details on our numerical experiments.

A Factor Directed Acyclic Graphs

In this section, we present general definitions and properties of Factor Directed Graphs.

A.1 Definitions

Let $d \in \mathbb{N}$ be the number of feature vertices and $m \in \mathbb{N}$ be the number of factor vertices. We start with a few definitions.

Definition 1. (*Factor Directed Graph*) Let $V = \{v_1, \dots, v_d\}$ denote the set of feature vertices (which we also call feature nodes, variable vertices, or variable nodes), and $F = \{f_1, \dots, f_m\}$ the set of factor vertices (or factor nodes). Let E be a set of directed edges, such that there are no edges between two nodes of same type (factors or features). We define a Factor Directed Graph (f -DiGraph) as the bipartite graph $G_f = (V, F, E)$.

Definition 2. (*Set of factor graphs with m modules and d nodes*) The subset of factor graphs \mathbb{G}_d^m with d variables and m factors is defined as:

$$\mathbb{G}_d^m = \{G_f \mid G_f = (V, F, E) \text{ is a factor directed graph and } |V| = d, |F| = m\}. \quad (9)$$

Definition 3. (*Half-square graphs and induced feature graph*) G_f canonically induces two half-square graphs $G_f^2[V]$ and $G_f^2[F]$. $G_f^2[V]$ is defined as the graph on V with an edge between two vertices of V if there is a path of length exactly two between these vertices in G_f . $G_f^2[F]$ is defined similarly on the nodes F . We specifically write $G = G_f^2[V]$ and refer to it as the feature graph (as opposed to the factor graph G_f).

Definition 4. (*Set of feature graphs with m modules and d nodes*) The set of feature graphs \mathcal{G}_d^m formed from half-square graphs with d variables and m factors is defined as:

$$\mathcal{G}_d^m = \{G = G_f^2[V] \mid G_f \in \mathbb{G}_d^m\}. \quad (10)$$

A.2 General properties

We start by outlining some general properties of f -DiGraphs. First, we observe that every graph may be written as the feature graph of a bipartite graph.

Proposition 2. (*Representation*) Let \mathcal{G} denote the set of all feature graphs, i.e., directed graphs on V . Then we have

$$\mathcal{G} = \bigcup_{m=1}^{\infty} \mathcal{G}_d^m. \quad (11)$$

Proof. By definition, we have that $\mathcal{G}_d^m \subset \mathcal{G}$ for all m , which proves the reverse set inclusion. Therefore, we focus on the direct set inclusion. Let $G = (V, E) \in \mathcal{G}$. We set $F = E$ and define the set of edges E' as

$$E' = \bigcup_{e=(v_1, v_2) \in E} \{(v_1, e), (e, v_2)\}. \quad (12)$$

Then, for the bipartite graph $G'_f = (V, F, E') \in \mathbb{G}_d^{|E|}$, we obtain $G'^2_f[V] = G$ as desired. \square

Second, we discuss the size of the set of DAGs within \mathcal{G}_d^m compared to \mathcal{G} . We start with a lemma for a fixed topological ordering σ .

Lemma 2. *Denote by \mathcal{D}_d the subset of acyclic graphs in \mathcal{G} with d nodes, and by \mathcal{D}_d^m the subset of acyclic graphs in \mathcal{G}_d^m . For σ , a permutation of $\{v_1, \dots, v_d\}$, we denote by $\mathcal{D}_d^m(\sigma)$ (resp. $\mathcal{D}_d(\sigma)$) the subset of graphs in \mathcal{D}_d^m (resp. \mathcal{D}_d) for which σ is a topological ordering. Then, we have:*

$$|\mathcal{D}_d(\sigma)| = 2^{\frac{d(d-1)}{2}}, \quad (13)$$

$$|\mathcal{D}_d^m(\sigma)| \leq \binom{d+m}{m} 2^{dm}. \quad (14)$$

Proof. If σ is a valid topological ordering for a graph, then its adjacency matrix is upper triangular (with zero on the diagonal) under this ordering of the rows and columns.

In the case of $\mathcal{D}_d(\sigma)$, we must simply count the number of binary matrices that are upper triangular with zeros on the diagonal. As such matrices have $\frac{d(d-1)}{2}$ entries potentially taking one of two values, this proves the first part of this proposition.

The case for $\mathcal{D}_d^m(\sigma)$ is slightly more technical. In this setting, we have d variable nodes, and m factors. We are able to arrange the factors in between the features to obtain all possible topological orderings of factor graphs compatible with σ ,

$$(v_1, \dots, v_{i_1}, f_1, v_{i_1+1}, \dots, v_{i_m}, f_m, v_{i_m+1}, \dots, v_d), \quad (15)$$

with $1 \leq i_1 < \dots < i_m \leq d$, where, without loss of generality, we assumed the identity permutation on factors and features separately. We note that there are $\binom{d+m}{m}$ such possible combinations.

For a fixed arrangement, we may now observe that a variable node v_a can only be connected to one or several factor nodes appearing before v_a in the topological ordering, and each factor node f_j may only be connected to one or several feature nodes appearing before f_j in the topological ordering. We define the number of such possible adjacency patterns as I .

More precisely, each factor vertex f_j has 2^{i_j} potential incoming edge patterns. Also, each feature vertex v_a appearing after f_j gives rise to 2^j potential edge patterns and there are $i_{j+1} - i_j$ such vertices. Therefore, writing $i_{m+1} = d$, we have:

$$\log_2 I = \sum_{j=1}^m i_j + \sum_{j=1}^m j(i_{j+1} - i_j) \quad (16)$$

$$= \sum_{j=1}^m i_j + \sum_{j=1}^{m-1} j i_{j+1} + dm - \sum_{j=1}^m j i_j \quad (17)$$

$$= dm + \sum_{j=1}^m i_j + \sum_{j=2}^m (j-1) i_j - \sum_{j=2}^m j i_j - i_1 \quad (18)$$

$$= dm + \sum_{j=1}^m i_j - \sum_{j=1}^m i_j + \sum_{j=2}^m j i_j - \sum_{j=2}^m j i_j \quad (19)$$

$$= dm. \quad (20)$$

Because several factor graphs may yield the same half-square graph, we only have an upper bound, as claimed,

$$|\mathcal{D}_d^m(\sigma)| \leq \binom{d+m}{m} 2^{dm}. \quad \square$$

We can use this lemma to prove the following bound for the cardinality of the entire set of graphs:

Proposition 3. *(Cardinality of Directed Acyclic Graphs and half-square of f-DAGs) Denote by \mathcal{D}_d the subset of acyclic graphs in \mathcal{G} with d nodes, and by \mathcal{D}_d^m the subset of acyclic graphs in \mathcal{G}_d^m . For $d \geq m$, we have the inequality*

$$\frac{|\mathcal{D}_d^m|}{|\mathcal{D}_d|} \leq \left(1 + \frac{d}{m}\right)^{m+1/2} \exp \left\{ -\frac{d^2}{2} + d \left(m \log 2 + \log(m+d) + \frac{\log 2}{2} - 1 \right) \right\} \quad (21)$$

$$\leq \exp \left\{ dm + 4d \log(m+d) - \frac{\log 2}{2} d^2 \right\}, \quad (22)$$

and therefore for fixed m , $\frac{|\mathcal{D}_d^m|}{|\mathcal{D}_d|} \rightarrow 0$ when $d \rightarrow +\infty$.

Proof. Let us first provide a (loose but sufficient) lower bound on $|\mathcal{D}_d|$. In the light of the previous result for a fixed permutation, there are at least $2^{\frac{d(d-1)}{2}}$ DAGs in $|\mathcal{D}_d|$.

Next, we want to establish an upper bound on $|\mathcal{D}_d^m|$. Because for each permutation σ , there are at most $|\mathcal{D}_d^m(\sigma)|$ distinct graphs, an upper bound on $|\mathcal{D}_d^m|$ is given by $d! \binom{d+m}{m} 2^{dm}$.

Putting this together, and using a non-asymptotic version of Stirling's formula, we obtain

$$\frac{|\mathcal{D}_d^m|}{|\mathcal{D}_d|} \leq \frac{(d+m)!}{m!} 2^{dm} 2^{-\frac{d(d-1)}{2}} \quad (23)$$

$$\leq \frac{\sqrt{2\pi(m+d)} (m+d/e)^{m+d}}{\sqrt{2\pi m} (m/e)^m} 2^{dm} 2^{-\frac{d(d-1)}{2}} e^{\frac{1}{12(m+d)} - \frac{1}{12m+1}} \quad (24)$$

$$\leq (m+d)^{m+d+\frac{1}{2}} 2^{dm-\frac{d(d-1)}{2}} \quad (25)$$

$$\leq \exp \left\{ \left(m+d+\frac{1}{2} \right) \log(m+d) + dm \log 2 - \frac{\log 2}{2} d^2 + \frac{d \log 2}{2} \right\} \quad (26)$$

$$\leq \exp \left\{ dm + 4d \log(m+d) - \frac{\log 2}{2} d^2 \right\} \quad (27)$$

if $d \geq m$. By comparing coefficients inside the exponential, for fixed m , this upper bound tends to 0 as $d \rightarrow \infty$. \square

A.3 Relationship to low-rank matrices

We now discuss properties of the mapping $\zeta : G_f \mapsto G = G_f^2[V]$ defined over the set of factor graphs.

First, we remark that, in general, ζ is not injective, as shown by the following counterexample.

Example 1. (*Induced half-square is not injective*) Let $V = \{v_1, v_2, v_3\}$ and $F = \{f_1, f_2\}$. Let $E_1 = \{(v_3, f_2), (v_3, f_1), (v_2, f_2)\} \cup \{(f_1, v_2), (f_2, v_1)\}$ and $E_2 = \{(v_3, f_2), (v_2, f_1)\} \cup \{(f_1, v_1), (f_2, v_1), (f_2, v_2)\}$. For $G_{f,1} = (V, F, E_1)$ and $G_{f,2} = (V, F, E_2)$, we have the identity $G_{f,1}^2[V] = G_{f,2}^2[V]$, in the sense that both graphs have the same set of vertices and edges.

Second, we characterize the image $\zeta(\mathbb{G}_d^m) = \mathcal{G}_d^m$ in terms of the Boolean rank of the associated adjacency matrices. Let us define the adjacency matrix $\mathcal{A}(G_f)$ of a factor graph $G_f \in \mathbb{G}_d^m$. Because the graph is bipartite, up to a permutation of the rows and columns, we may write it in block form,

$$\mathcal{A}(G_f) = \begin{bmatrix} \mathbf{0}_{d \times d} & \mathbf{U} \\ \mathbf{V} & \mathbf{0}_{m \times m} \end{bmatrix}, \quad (28)$$

where $\mathbf{U} \in \mathbb{R}^{d \times m}$ (resp. $\mathbf{V} \in \mathbb{R}^{m \times d}$) denotes the binary matrix encoding the presence or absence of edges towards factor nodes (resp. variable nodes) according to the edge set E . We now relate these two matrices to the adjacency matrix of the half-square graph.

Proposition 1 (Bounded Boolean rank of half-square adjacency matrix). *For a factor graph $G_f = (V, F, E)$, let $\mathbf{U} \in \{0, 1\}^{d \times m}$ (resp. $\mathbf{V} \in \{0, 1\}^{m \times d}$) be the binary matrix encoding the presence or absence of edges directed towards factor nodes (resp. variable nodes), according to E . The adjacency matrix $\mathcal{A}(G)$ of the half-square graph G may be decomposed as $\mathcal{A}(G) = \mathbf{U} \diamond \mathbf{V}$ where \diamond denotes the Boolean matrix product, $(\mathbf{U} \diamond \mathbf{V})_{ij} = \bigvee_{k=1}^m \mathbf{U}_{ik} \wedge \mathbf{V}_{kj}$, $i, j \in [d]$. Consequently, $\mathcal{A}(G)$ has Boolean rank bounded above by m . Conversely, every adjacency matrix over the feature nodes with Boolean rank bounded by m can be written as half-square of an f -DiGraph with m factors.*

Proof. Let G_f be a factor graph, and let \mathbf{U} and \mathbf{V} be defined as in (28). The adjacency matrix $\mathcal{A}(G)$ of the half-square graph $G = G_f^2[V]$ can be calculated as

$$\forall (i, j) \in [d]^2, \quad \mathcal{A}(G)_{ij} = \bigvee_{k=1}^m \mathbf{U}_{ik} \wedge \mathbf{V}_{kj}, \quad (29)$$

where \wedge and \vee denote the logical AND and OR operators, respectively.

Indeed, by definition, there is an edge between two nodes v_a and v_b of G if and only if there exists a path of length two between those two nodes in G_f . Because edges may exist only between factor and feature nodes, this condition is met if and only if there exists an edge between v_a and f as well as f and v_b for at least one factor node f .

This proves that every adjacency matrix of a graph in \mathcal{G}_d^m can be written as the matrix product of a $d \times m$ and a $m \times d$ matrix for the Boolean arithmetic. By definition [29], $\mathcal{A}(G)$ therefore has Boolean rank bounded above by m .

The converse follows by observing that, by definition, an adjacency matrix with Boolean rank bounded above by m admits the decomposition (29) with binary matrices \mathbf{U} , \mathbf{V} . Defining an f -DiGraph with these adjacency matrices according to (28) yields the claim. \square

For one direction of Proposition 1, we have a similar result for the weighted adjacency matrices \mathbf{UV} .

Proposition 4 (Bounded rank of weighted half-square adjacency matrix). *For a factor graph G_f and matrices \mathbf{U} and \mathbf{V} , the (regular matrix) product \mathbf{UV} counts the number of paths of length two between two variable nodes in G_f , and therefore is a valid (weighted) adjacency matrix for $G = G_f^2[V]$. Additionally, \mathbf{UV} has matrix rank bounded above by $\min(d, m)$.*

Proof. Replacing \vee by $+$ and \wedge by \times in (29), we obtain the matrix product \mathbf{UV} . Because of this, individual entries in the matrix \mathbf{UV} indeed count the number of distinct paths of length two between two feature nodes in G_f . As a consequence, \mathbf{UV} has a zero entry if and only if $\mathcal{A}(G)$ has a zero entry. This proves that \mathbf{UV} is a valid weighted adjacency matrix. By construction, its matrix rank is bounded above by $\min(d, m)$. \square

A.4 Alternate definitions of low-rank graphs

Here, we introduce various notions of low-rank constraints on graphs, and make precise the class we are concerned with in this paper. Towards this end, one could consider a variety of subsets of \mathcal{G} , the set of all graphs on d nodes, in particular:

1. $\mathcal{G}_{\text{lin}}^m$: graphs that admit a weighted adjacency matrix W that has a matrix factorization of rank $\leq m$.
2. $\mathcal{G}_{\text{lin,nonneg}}^m$: graphs that admit a weighted adjacency matrix W that has a non-negative matrix factorization of rank $\leq m$.
3. $\mathcal{G}_{\text{bool}}^m$: graphs that admit a weighted adjacency matrix W that has a Boolean matrix factorization of rank $\leq m$.

Note that in the definition of $\mathcal{G}_{\text{lin}}^m$, we allow for W to encode the presence of an edge in G with any non-zero entry, positive or negative. In this context, we have the following set inclusions:

$$\mathcal{G}_{\text{bool}}^m = \mathcal{G}_{\text{lin,nonneg}}^m \not\subseteq \mathcal{G}_{\text{lin}}^m \not\subseteq \mathcal{G}, \quad (30)$$

for $m < d$. To understand this result, it is important to note that for a given matrix, its non-negative rank and Boolean rank do not necessarily coincide, but $\mathcal{G}_{\text{bool}}^m = \mathcal{G}_{\text{lin,nonneg}}^m$ since we allow for arbitrary weighted adjacency matrices in the definition of $\mathcal{G}_{\text{lin,nonneg}}^m$.

The previous low-rank work [20] searches for graphs in $\mathcal{G}_{\text{lin}}^m$. By contrast, we do not consider $\mathcal{G}_{\text{lin}}^m$, but instead choose to exclusively work with $\mathcal{G}_{\text{bool}}^m$. Considering $\mathcal{G}_{\text{bool}}^m$ instead of $\mathcal{G}_{\text{lin}}^m$ gives further rise to an intuitive way of restricting the nonlinear functional relationships on top of the graphical structure while maintaining low asymptotic computational complexity, as presented in Section 4. Besides being more immediate when starting from a linear structural equation model, we see no particular reason for favoring $\mathcal{G}_{\text{lin}}^m$ over $\mathcal{G}_{\text{bool}}^m$ in light of the practical benefits outlined in the later sections of this paper. Moreover, the only linear low-rank models not captured in $\mathcal{G}_{\text{bool}}^m$ are those in which the contributions of multiple factors cancel out to produce more zeros than expected from the sparsity pattern of the factors U, V , corresponding to a lack of faithfulness of the factor graph. We consider these models edge cases that could safely be excluded from the search space.

B Identifiability of f -DAGs

In this section, we investigate the identifiability of Factor Directed Acyclic Graphs from observational data in the context of causal discovery. We first define the concept of Markov Equivalence Class (MEC), and we introduce a Boolean-rank restricted equivalence class. We show that the latter is in general smaller (and sometimes strictly smaller) than the MEC.

B.1 Markov equivalence classes

Under the classical set of assumptions commonly employed in causal discovery, namely causal sufficiency, causal Markov property, and faithfulness, we may identify the causal DAG from observational data only up to its Markov Equivalence Class (MEC) [59]:

Definition 5. (*Markov Equivalence Class*) The MEC of the half-square graph $D \in \mathcal{D}_d^m$ is $M(D) = \{D' \mid D' \sim D\}$ where \sim denotes Markov equivalence.

A graphical rule for Markov equivalence is that two graphs are Markov equivalent if they share the same skeleton and v-structures [59]. Ideally, we wish to characterize the complexity of searching for a DAG only in a subset of the Markov equivalence class that is composed of graphs in \mathcal{D}_d^m .

Definition 6. (*f -MEC*) The f -MEC $M_f^m(D)$ of a half-square graph $D \in \mathcal{D}_d^m$ is the set of DAGs that are Markov equivalent to D and arise as the half-square of a factor graph with at most m factors: $M_f^m(D) = M(D) \cap \mathcal{D}_d^m$.

We represent a MEC with an essential graph, defined as the union of all vertices and edges in the MEC. In particular, we say that an edge is unoriented if there exists an edge and its reverse orientation in the MEC.

Although by definition, we have the inclusion $M_f^m(D) \subset M(D)$, it is worth noting that this inclusion is in general not equal.

Example 2. Let $V = \{v_1, v_2, v_3\}$, $F = f_1$ and $E = \{(v_3, f_1), (f_1, v_1), (f_1, v_2)\}$. The graph $G_f = (V, F, E)$ is a valid factor graph with one factor. The half-square graph G has two edges $\{(v_3, v_1), (v_3, v_2)\}$ that are both unoriented for the (classical) Markov equivalence class. Indeed, $M(G)$ contains three graphs, obtained by flipping edges (except for the configuration that creates a v-structure). However, $M_f^1(G)$ has only a unique graph, because the two other graphs in $M(G)$ require two factors when being described as a factor graph.

We leave the problem of providing an algebraic characterization of an f -MEC as future work.

B.2 Identifiability of Boolean low-rank graphs

Because graphs in \mathcal{D}_d^m potentially contain many v-structures, we obtain a simple condition for identifiability.

Lemma 3. (*Unoriented edges in Boolean low-rank graphs*) Let $D_f = (V, F, E)$ be an f -DAG and $D = D_f^2[V] \in \mathcal{D}_d^m$. For every unoriented edge (v_i, v_j) in the essential graph of D , there exists a factor f with unique parent v_i . Consequently, if every factor $f \in F$ has at least two parents in D_f , then the MEC of D reduces to the singleton $\{D\}$.

Proof. Let D_f be a factor directed graph such that $D = D_f^2[V]$. Let (v_i, v_j) be an edge of D_f that is unoriented in $M(D)$. By definition of the factor directed graph, there exists $f \in \mathcal{F}$ such that the edges (v_i, f) and (f, v_j) are part of \mathcal{G} . Because the edge is unoriented, it cannot be part of a v-structure. Consequently, there are no other feature vertices v_k connected to f or it would create a v-structure in D .

In the case that every factor $f \in \mathcal{F}$ has at least two parents, there can be no unoriented edges, and therefore the graph is identifiable, i.e., it is alone in its MEC. \square

In order to quantify how frequent this configuration is, we introduce a random factor directed acyclic graph model, inspired by the Erdős-Rényi model [36]:

Definition 7. (Random sequence of growing f -DAGs) Let $(D_{f,d})_{d=0}^{\infty}$ denote a random sequence of factor directed graphs defined recursively, with $D_{f,0} = (\emptyset, F, \emptyset)$ and $|F| = m$. Let $D_{f,d} = (V_d, F, E_d)$ be the graph at step d , and σ_d a permutation of $F \cup V_d$ that specifies a topological ordering $\{\sigma(v_1), \dots, \sigma(v_d)\}$. We define $V_{d+1} = V_d \cup \{v_{d+1}\}$ where v_{d+1} denotes a new variable node. We extend the permutation σ_d into a new permutation σ_{d+1} of $F \cup V_{d+1}$ by randomly inserting the node v_{d+1} into the linear order induced by σ_d (out of the $d + m + 1$ possible choices). To obtain E_{d+1} , we add to E_d edges of the form (v_{d+1}, f) (resp. (f, v_{d+1})) if $(\sigma(v_{d+1}) \leq \sigma(f))$ (resp. $(\sigma(f) \leq \sigma(v_{d+1}))$) independently with probability $p \in (0, 1)$. Finally, we define $D_{f,d+1} = (V_{d+1}, F, E_{d+1})$ and have $D_{d+1} = D_{f,d+1}^2[V] \in \mathcal{D}_{d+1}^m$.

We show that the probability of having at least one unoriented edge in $M(D_d)$ for a fixed m is small for large d .

Proposition 5. For D_d sampled according to Definition 7, the size of the MEC (and, by inclusion, of the f -MEC) converges to 1 with high probability for fixed m :

$$\mathbb{P}(|M(D_d)| = 1) \geq 1 - \phi(d, m, p), \quad (31)$$

with $\phi(d, m, p) \rightarrow 1$ when p and m are fixed, and $d \rightarrow \infty$. Consequently, as the number of variable nodes d grows, the DAG becomes identifiable.

Proof. According to the graphical rule in Lemma 3, if all factors $f \in F$ have at least two parents then the MEC $M(D_n)$ of the DAG D_n reduces to a singleton $\{D_n\}$. Consequently, we have the lower bound

$$\mathbb{P}(|M(D_d)| = 1) \geq \mathbb{P}(\forall f \in F : |\text{Pa}(f)| \geq 2). \quad (32)$$

Calculating the right-hand side of the previous inequality essentially corresponds to calculating the distribution of the number of parents $|\text{Pa}(f)|$ for each factor f . To bound this probability, we first note that we can obtain the probability distribution (on graphs) in Definition 7 equivalently by fixing an order on the feature nodes and inserting m factor nodes randomly, one by one, into the order, finally assigning edges independently as before. In this construction, for each factor f , the number of preceding feature nodes and the number of parents are independent. The number of parents follows a binomial distribution with parameters (K_f, p) where K_f is the number of feature nodes K_f appearing before f in the topological ordering σ_d . By construction, K_f is independently sampled from a uniform distribution $K_f \sim \text{Categorical}(\{0, \dots, d\})$. Therefore, it follows that

$$\mathbb{P}(\forall f \in F : |\text{Pa}(f)| \geq 2) = [\mathbb{P}(\text{a fixed } f \in F \text{ verifies } |\text{Pa}(f)| \geq 2)]^m \quad (33)$$

$$= [1 - \mathbb{P}(\text{a fixed } f \in F \text{ verifies } |\text{Pa}(f)| \in \{0, 1\})]^m \quad (34)$$

$$\geq 1 - m\mathbb{P}(A_d), \quad (35)$$

where we introduce the probabilistic event $A_d = \{\text{a fixed } f \in F \text{ verifies } |\text{Pa}(f)| \in \{0, 1\}\}$. Then, conditioning on K_f , we obtain

$$\mathbb{P}(A_d) = \frac{1}{d+1} \sum_{k=0}^d [(1-p)^k + kp(1-p)^{k-1}] \quad (36)$$

$$= \frac{1}{d+1} \sum_{k=0}^d (1-p)^k + \frac{p}{(d+1)(1-p)} \sum_{k=0}^d k(1-p)^k \quad (37)$$

$$= \frac{1 - (1-p)^{d+1}}{(d+1)p} + \frac{p}{(d+1)(1-p)} \left[\frac{1-p}{p^2} (1 - (1-p)^{d+1}) - \frac{d+1}{p} (1-p)^{d+1} \right] \quad (38)$$

$$= \frac{2(1 - (1-p)^{d+1})}{(d+1)p} - (1-p)^d, \quad (39)$$

where we recognized the closed-form expression of a geometric series, and a finite arithmetico-geometric series, respectively. Hence, because $\mathbb{P}(A_d) \rightarrow 1$ when $d \rightarrow \infty$, we have that $\mathbb{P}(|M(D_d)| = 1) \rightarrow 1$ when $d \rightarrow \infty$. \square

B.3 Empirical validation

To simulate f -DAGs, we used a random graph model equivalent to Definition 7 and specified as follows. For d variable nodes and m factor nodes, we sample a random permutation σ that specifies a

topological ordering on $[d + m]$. For each node i in this topological ordering $\{\sigma(1), \dots, \sigma(d + m)\}$, we draw the absence or the presence of an edge between node i and each of its potential parents based on a Bernoulli distribution. If node i is a variable node, then it may only be connected to factors present in $\{\sigma(1), \dots, \sigma(i)\}$ with probability p_v . Similarly, if node i is a factor node, then it may only be connected to factors present in $\{\sigma(1), \dots, \sigma(i)\}$ with probability p_f . This is a natural extension of the simulations provided in [6], further adding the factor semantic.

Using this framework, we sampled $T = 50$ f -DAGs with d nodes and m modules ($p_v = p_f = 0.5$), and calculated the size of the MEC using the causaldag Python package (Figure 2A).

C Boolean-rank instability under edge perturbation

In this section, we prove the Boolean-rank instability result (Theorem 1). The key idea behind the proof is to identify a sufficient condition for the perturbation to induce a Boolean rank increase in the half-square graph that happens often for large d and fixed m . The proof consists of four parts. First, we introduce a technical lemma regarding the overlap of random sets. Namely, any pair of distinct union of sets of random subsets from an alphabet differ in at least two elements with high probability (Lemma 4). Second, we introduce another lemma showing that the sampling of patterns in a binary vector becomes exhaustive after enough independent draws (Lemma 5). Third, we relate those two conditions to a sufficient condition for the increase of the Boolean rank of the half-square of a f -DiGraph (Lemma 6). Putting everything together, we finally prove the main theorem (Theorem 1).

C.1 Random subset non-overlapping lemma

Lemma 4. *Let $\{\mathcal{U}_1, \dots, \mathcal{U}_m\}$ be m random subsets of the alphabet $\Omega = [d]$, where the inclusion of each letter $i \in \Omega$ in each subset $\mathcal{U}_k \subset \Omega$ for $k \in [m]$ is defined by sampling a Bernoulli random variable with parameter p , independently over $k \in [m]$ and $i \in [d]$. Further, let $S_1 \neq S_2$ be two distinct fixed subsets of $[m]$. Then, the two sets defined as the unions of subsets of $\{\mathcal{U}_1, \dots, \mathcal{U}_m\}$ indexed by S_1 and S_2 have low probability of completely overlapping:*

$$\mathbb{P}\left(\left|\left(\bigcup_{j \in S_1} \mathcal{U}_j\right) \Delta \left(\bigcup_{j' \in S_2} \mathcal{U}_{j'}\right)\right| \leq 1\right) \leq \gamma q_A^d, \quad (40)$$

where Δ denotes the symmetric set difference, $\gamma = 1 + d/(1-p(1-p)^m) > 0$, and $q_A = 1 - p(1-p)^m \in (0, 1)$.

Proof. We introduce $X_w^{S_i}$, the random variable that denotes whether letter $w \in \Omega$ is present in $\bigcup_{j \in S_i} \mathcal{U}_j$. We observe that a letter w gives rise to an element in the symmetric difference of the two sets S_1 and S_2 if $X_w^{S_1} \neq X_w^{S_2}$. Although the sets $\{\mathcal{U}_1, \dots, \mathcal{U}_m\}$ are constructed independently, there may be correlations in the union sets we consider in the case of overlap between S_1 and S_2 . Therefore, we decompose the sets S_1 and S_2 into their overlapping and non-overlapping parts:

$$S_1 = S'_1 \sqcup S_3 \quad (41)$$

$$S_2 = S'_2 \sqcup S_3, \quad (42)$$

where \sqcup denotes a disjoint union, $S_3 = S_1 \cap S_2$, $S'_1 = S_1 \setminus S_3$ and $S'_2 = S_2 \setminus S_3$. Under these conditions, we may write

$$A_w := \{X_w^{S_1} \neq X_w^{S_2}\} = \underbrace{\left\{w \in \bigcup_{j \in S_1} \mathcal{U}_j \cap w \notin \bigcup_{j \in S_2} \mathcal{U}_j\right\} \cup \left\{w \in \bigcup_{j \in S_2} \mathcal{U}_j \cap w \notin \bigcup_{j \in S_1} \mathcal{U}_j\right\}}_{=: \bar{A}_w}. \quad (43)$$

Noticing that these events are symmetric in S_1 and S_2 , we focus on the first one which we denote by \bar{A}_w . In each of the above events, w cannot be in the union over S_3 because in that case, it would be in the union over both S_1 and S_2 . Therefore, we can decompose \bar{A}_w as

$$\bar{A}_w = \{w \in \bigcup_{j \in S'_1} \mathcal{U}_j\} \cap \{w \notin \bigcup_{j \in S'_2} \mathcal{U}_j\} \cap \{w \notin \bigcup_{j \in S_3} \mathcal{U}_j\}. \quad (44)$$

By the independence of $\{\mathcal{U}_1, \dots, \mathcal{U}_m\}$, we have that

$$\mathbb{P}(\bar{A}_w) = \left(1 - (1-p)^{|S'_1|}\right) (1-p)^{|S'_2|} (1-p)^{|S_3|} \quad (45)$$

$$= \left(1 - (1-p)^{|S'_1|}\right) (1-p)^{|S_2|}. \quad (46)$$

Then, because $|S'_1|, |S_2| \in \{0, \dots, m\}$, we have the bound

$$\mathbb{P}(A_w) \geq \mathbb{P}(\bar{A}_w) \geq p(1-p)^m. \quad (47)$$

Now, noting the independence of the letters, we have that

$$\mathbb{P}\left(\left|\left(\bigcup_{j \in S_1} \mathcal{U}_j\right) \Delta \left(\bigcup_{j' \in S_2} \mathcal{U}_{j'}\right)\right| \leq 1\right) = \mathbb{P}(\text{At most one } A_w \text{ is true}) \quad (48)$$

$$= (1 - \mathbb{P}(A_w))^d + d\mathbb{P}(A_w)(1 - \mathbb{P}(A_w))^{d-1} \quad (49)$$

$$\leq (1 - \mathbb{P}(A_w))^d + d(1 - \mathbb{P}(A_w))^{d-1} \quad (50)$$

$$\leq (1 - p(1-p)^m)^d + d(1 - p(1-p)^m)^{d-1} \quad (51)$$

$$\leq \left(1 + \frac{d}{1 - p(1-p)^m}\right) (1 - p(1-p)^m)^d. \quad (52)$$

This concludes the proof. \square

C.2 Exhaustive binary pattern coverage lemma

Lemma 5. Let $\mathcal{V} = [v_1, \dots, v_m] \in \{0, 1\}^m$ be a random vector with each entry independently sampled from a Bernoulli distribution with parameter p . Denote by B the following probabilistic event:

$$B = \{\exists x \in \{0, 1\}^m \text{ that is not observed at least twice in } d \text{ independent draws from } \mathcal{V}\}.$$

Then, the probability of B is small for large d , in particular,

$$\mathbb{P}(B) \leq \delta q_B^d \quad (53)$$

with $\delta = 2^m \left(1 + \frac{d}{1 - \max\{p^m, (1-p)^m\}}\right)$ and $q_B = 1 - \min\{p^m, (1-p)^m\} \in (0, 1)$.

Proof. By a union bound, we obtain

$$\mathbb{P}(B) = \mathbb{P}(\exists x \in \{0, 1\}^m : x \text{ appears at most once in } d \text{ draws}) \quad (54)$$

$$\leq 2^m \max_{x \in \{0, 1\}^m} \mathbb{P}(\text{a fixed } x \in 2^m \text{ appears at most once in } d \text{ draws}). \quad (55)$$

We simply need to upper bound this probability. For a fixed $x \in \{0, 1\}^m$, denote by $|x|$ the number of non-zero entries in the binary vector x . We then have, by independence:

$$\mathbb{P}(\text{a fixed } x \in 2^m \text{ appears at most once in } d \text{ draws}) = (1 - p_x)^d + dp_x(1 - p_x)^{d-1}, \quad (56)$$

where

$$p_x = p^{|x|} (1-p)^{m-|x|} \in (p_\beta, p_\alpha), \quad (57)$$

with $p_\alpha = \max\{p^m, (1-p)^m\}$ and $p_\beta = \min\{p^m, (1-p)^m\}$. This inequality directly follows from distinguishing the cases $p \leq 1/2$ and $p > 1/2$. Plugging this into the first bound above, we have

$$\mathbb{P}(B) \leq 2^m \left(1 + \frac{d}{1 - p_\alpha}\right) (1 - p_\beta)^d, \quad (58)$$

which concludes the proof. \square

C.3 Boolean rank increase lemma

Lemma 6. Let $G_f \in \mathcal{G}_d^m$ be a (fixed) f -DiGraph, with partial adjacency matrices \mathbf{U} and \mathbf{V} . We denote by G its half-square $G = G_f^2[V]$. Let us state two assumptions.

First, we say that the matrix \mathbf{U} satisfies the non-overlapping condition if

$$\forall (x_1, x_2) \in \{0, 1\}^m, x_1 \neq x_2 \implies d_{\mathcal{H}}(\mathbf{U} \diamond x_1, \mathbf{U} \diamond x_2) \geq 2 \quad (\text{non-overlap})$$

where $d_{\mathcal{H}}$ denotes the Hamming distance between two binary vectors.

Second, we say that the matrix \mathbf{V} satisfies the coverage condition if its columns cover the whole set of possible patterns at least twice, i.e.,

$$\forall x \in \{0, 1\}^m \exists i_1 \neq i_2 \in [d] : \mathbf{V}_{:,i_1} = \mathbf{V}_{:,i_2} = x. \quad (\text{coverage})$$

If both conditions are satisfied for \mathbf{U} and \mathbf{V} , resp., then the adjacency matrix $\mathbf{A} = \mathbf{U} \diamond \mathbf{V}$ of the half-square graph G has 2^m distinct columns (treated as binary vectors), and \mathbf{A} has Boolean rank m . Moreover, for every entry (i, j) of the adjacency matrix, the matrix \mathbf{A}' obtained by replacing $(\mathbf{U} \diamond \mathbf{V})_{ij}$ by $1 - (\mathbf{U} \diamond \mathbf{V})_{ij}$ has Boolean rank $m + 1$.

Proof. The reader will notice that (non-overlap) for \mathbf{U} in this lemma is a matrix formulation of the hypothesis in lemma 4 for all sets $S_1, S_2 \subseteq [m]$, and that (coverage) for \mathbf{V} is a direct reformulation of the hypothesis in lemma 5.

Let us note that one consequence of (non-overlap) is that two different patterns in the columns of \mathbf{V} will incur different patterns in the columns of \mathbf{A} (the Hamming distance is bounded away from zero). Also, as a consequence of (coverage), we know that each pattern occurs at least once, and therefore the matrix \mathbf{A} has 2^m distinct columns. Because at least m factors in a Boolean decomposition are necessary to express 2^m distinct column patterns, \mathbf{A} is of Boolean rank m [60].

To show the second claim, for a fixed entry of the adjacency matrix, let (i, j) be its indices. We replace $(\mathbf{U} \diamond \mathbf{V})_{ij}$ by $1 - (\mathbf{U} \diamond \mathbf{V})_{ij}$ in \mathbf{A} to create \mathbf{A}' . By (non-overlap), the j th column of \mathbf{A}' is distinct from all other columns in \mathbf{A}' , since it differs in exactly one entry from all the other columns, but these columns have a Hamming distance of at least two from each other. Moreover, since every pattern occurs at least twice in \mathbf{A} by (coverage), all 2^m original column patterns in \mathbf{A} are still present in \mathbf{A}' . Therefore, \mathbf{A}' has $2^m + 1$ distinct columns. By the same argument as above, at least $m + 1$ factors are necessary to express \mathbf{A}' with a Boolean decomposition, and thus $\text{Rank}_{\mathcal{B}}(\mathbf{A}') = m + 1$. \square

C.4 Proof of the main theorem

We introduce a random factor graph model over \mathcal{G}_d^m , inspired by the Erdős-Rényi model [36]:

Definition 8. (Random sequence of growing f -DiGraphs) Let $(G_{f,d})_{d=0}^{\infty}$ denote a random sequence of factor directed graphs defined recursively, with $G_{f,0} = (\emptyset, F, \emptyset)$. Let $G_{f,d} = (V_d, F, E_d)$ be the graph at step d . We define $V_{d+1} = V_d \cup \{v_{d+1}\}$ where v_{d+1} denotes a new variable node. To obtain E_{d+1} , we connect the new variable node into and out of each factor independently with probability $p \in (0, 1)$. Finally, we define $G_{f,d+1} = (V_{d+1}, F, E_{d+1})$ and have $G_{d+1} = G_{f,d+1}^2[V] \in \mathcal{G}_{d+1}^m$.

The reader will note that those graphs are not necessarily acyclic, but our result for the Boolean rank is true for the more general class of f -DiGraphs under this model. We now introduce our toy model for edge perturbations.

Definition 9. (Stochastic edge operator) Let $G \in \mathcal{G}_d^m$. We denote by Λ the stochastic operator that samples a random entry of the adjacency matrix $\mathcal{A}(G)$ and either removes the present edge, or adds the absent edge.

Theorem 1 (Boolean rank instability for edge perturbation). Let $G \in \mathcal{G}_d^m$ be sampled according to an Erdős-Rényi random directed graph model. The probability that adding or removing an edge increases the Boolean rank is arbitrarily high for large d :

$$\mathbb{P}(\text{Rank}_{\mathcal{B}}(\Lambda(G)) > \text{Rank}_{\mathcal{B}}(G)) \geq 1 - \alpha q^d, \quad (5)$$

where $\text{Rank}_{\mathcal{B}}$ denotes the Boolean rank, and $\alpha > 0$ and $q \in (0, 1)$ depend on m and the parameters of the random graph model.

Proof. Let us denote the rank increase event by $R = \{\text{Rank}_B(\Lambda(G_d)) > \text{Rank}_B(G_d)\}$. Thanks to Lemma 6, if the random matrices \mathbf{U} and \mathbf{V} corresponding to G fulfill (non-overlap) and (coverage), the rank increases no matter which edge is flipped due to Λ . Therefore, we have

$$\mathbb{P}(\bar{R}) \leq \mathbb{P}(\{\text{not (non-overlap)}\} \text{ or } \{\text{not (coverage)}\}) \quad (59)$$

$$\leq \mathbb{P}(\{\text{not (non-overlap)}\}) + \mathbb{P}(\{\text{not (coverage)}\}) \quad (60)$$

$$\leq \mathbb{P}\left(\bigcup_{S_1, S_2} \{ |(\cup_{j \in S_1} \mathcal{U}_j) \Delta (\cup_{j' \in S_2} \mathcal{U}_{j'})| \leq 1 \}\right) + \mathbb{P}(\{\text{not (coverage)}\}) \quad (61)$$

$$\leq 2^{2m} \mathbb{P}(\text{for fixed } S_1, S_2 : |(\cup_{j \in S_1} \mathcal{U}_j) \Delta (\cup_{j' \in S_2} \mathcal{U}_{j'})| \leq 1) + \mathbb{P}(\{\text{not (coverage)}\}) \quad (62)$$

$$\leq 2^{2m} \gamma q_A^d + \delta q_B^d \quad (63)$$

$$\leq (2^{2m} \gamma + \delta) (\max\{q_A, q_B\})^d, \quad (64)$$

where we used union bounds and Lemmas 4 and 5 to bound the probabilities. Folding the linear dependence of γ and δ on d into the exponential term q^d then concludes the proof. \square

C.5 Empirical validation

We simulated f -DAGs using the same methodology presented in Appendix B.3 with $p_v = p_f = 0.5$.

Boolean rank For each combination of $d \in \{10, 20, \dots, 90, 100\}$ and $m \in \{5, 10\}$, we simulated $T = 2$ f -DAGs. In the first simulation, we added an edge at random. In the second, we removed an edge at random. In Figure 2B, we calculated the Boolean rank of the adjacency matrix of the half-square graph G before and after perturbation, using the methodology and the code from [40] to approach the NP-hard problem of Boolean matrix factorization. More precisely, [40] provide a solver for the best Boolean rank \tilde{m} approximation of a matrix \mathbf{A} in Frobenius norm. Starting from the linear rank of the matrix \mathbf{UV} as an initial guess, we repeatedly used this solver to obtain the smallest \tilde{m} that resulted in a Frobenius norm residual of 0, i.e., perfect matrix reconstruction using \tilde{m} factors. After edge perturbation, we re-ran the solver and classified the graph as leading to a rank increase if the residual was 1 and as not leading to a rank increase if the residual was 0. Intuitively, an error of 1 means that the new edge cannot be described by any set of \tilde{m} factors, and an error of 0 means that a (potentially different) factorization with \tilde{m} factors reconstructs the perturbed graph.

Out of the 400 simulations, there were two configurations where the resulting residual was neither 0 nor 1. In both cases, the algorithm had not converged in time, and we excluded these two runs from the analysis. We found that the fraction of these suboptimal factorizations increased rapidly for larger m and therefore limited the analysis to small values of m .

Matrix rank For larger values of m , we calculated the linear rank of the (binary) adjacency matrix of the perturbed graph. We note that the linear rank is only a heuristic approximation of the quantitative increase in complexity of the underlying matrix, because in general it provides neither an upper nor a lower bound on the Boolean rank [41]. In this scenario, we chose a ratio of edges to perturb in the half-square graph $G = (V, E)$, given by the target False Discovery Rate (FDR) q . Out of these $q|E|$ corruptions, we sampled a number $N_1 = \text{Binomial}(q|E|, 1/2)$ of edges present in G uniformly at random to remove from the graph, and $N_2 = q|E| - N_1$ of edges not present in G uniformly at random to add. Then, we reported the linear rank before and after perturbations for $T = 200$ configurations for every target FDR.

D Characterization of acyclicity

We start by proving the graphical rule for acyclicity emerging from the structure of the bipartite graph.

Lemma 1 (Induced acyclicity). *Let $G = (V, F, E)$ be an f -DiGraph. Then,*

$$G_f \text{ is acyclic} \Leftrightarrow G = G_f^2[V] \text{ is acyclic} \Leftrightarrow G_f^2[F] \text{ is acyclic.} \quad (6)$$

Proof. To prove this, by symmetry between the sets of nodes F and V , it is enough to prove the first equivalence. We prove each implication of the first equivalence by contraposition.

Let us first assume that there exists a cycle in G_f , that is, that there exists a path starting and ending at the same node. That node is either a feature node or a factor node. If the node is a feature node v , then we may write the path as $[(v, f_{i_1}), (f_{i_1}, v_{j_1}), \dots, (v_{j_{\omega-1}}, f_{i_\omega}), (f_{i_\omega}, v)]$. By definition of the half-square, all feature nodes in this path are directly connected by at least one factor node. Therefore, the sequence $[(v, v_{j_1}), \dots, (v_{j_{\omega-1}}, v)]$ is a path in G . However, this path links v to itself, so it is a cycle. If the node is a factor, we may simply shift the cycle one step to obtain a path that starts from a feature node.

Let us now assume that there exists a cycle in G , for example $[(v, v_{j_1}), \dots, (v_{j_{\omega-1}}, v)]$. For every edge in G , there is by definition an edge of length 2 in G_f . Consequently, for every edge $(v_{j_a}, v_{j_{a+1}})$ of the path in G , there exists a path of length 2 $(v_{j_a}, f), (f, v_{j_{a+1}})$ in G_f connecting v_{j_a} and $v_{j_{a+1}}$. By concatenating these paths, we obtain a cycle in G_f . \square

We also note the existence of a more algebraic proof, based on the two following arguments. First, notice that for a matrix $W \in \mathbb{R}_+^{n \times n} = UV$, where all entries of U and V are also non-negative, W is nilpotent if and only if W is a DAG. Second, VU is nilpotent if and only if UV is nilpotent.

D.1 Trace-exponential characterization

Interestingly, in the case of an f -DiGraph G_f , we can be more precise, and prove that the tr-exp penalty applied to G can be related to the one applied to $G_f^2[F]$.

Proposition 6 (Tr exp penalty on f -DiGraphs). *Let $G_f = (V, F, E)$ be an f -DiGraph, and (\mathbf{U}, \mathbf{V}) its partial adjacency matrices. Then, the two following quantities are identical,*

$$\text{Tr exp}\{\mathbf{UV}\} - d = \text{Tr exp}\{\mathbf{VU}\} - m, \quad (65)$$

and are both equal to zero if and only if G_f or, equivalently, any of its half-squares, is acyclic.

Proof. Because \mathbf{UV} is a positively weighted adjacency matrix for G , we have that $\text{Tr exp}\{\mathbf{UV}\} = d$ if and only if G is acyclic [19]. Similarly, $\text{Tr exp}\{\mathbf{VU}\} = m$ if and only if $G_f^2[F]$ is acyclic. Considering the equivalences of acyclicity in Proposition 1, we must only prove the algebraic identity. For this, we write

$$\text{Tr exp}\{\mathbf{UV}\} - d = \text{Tr} \left[\sum_{k=0}^{\infty} \frac{(\mathbf{UV})^k}{k!} \right] - d \quad (66)$$

$$= \sum_{k=1}^{\infty} \frac{\text{Tr}[(\mathbf{UV})^k]}{k!} \quad (67)$$

$$= \sum_{k=1}^{\infty} \frac{\text{Tr}[\mathbf{U}(\mathbf{VU})^{k-1}\mathbf{V}]}{k!} \quad (68)$$

$$= \sum_{k=1}^{\infty} \frac{\text{Tr}[(\mathbf{VU})^{k-1}\mathbf{VU}]}{k!} \quad (69)$$

$$= \sum_{k=1}^{\infty} \frac{\text{Tr}[(\mathbf{VU})^k]}{k!} \quad (70)$$

$$= \text{Tr exp}\{\mathbf{VU}\} - m, \quad (71)$$

where we made use of the fact that $\text{Tr}(\mathbf{AB}) = \text{Tr}(\mathbf{BA})$. \square

D.2 Spectral characterization

We present here a version of the power iteration method tailored to the case of f -DiGraphs. It calculates an approximation to the spectral radius of \mathbf{UV} , in turn approximately characterizing acyclicity of the corresponding graph G (as presented in [26]).

Algorithm 1 Factor power iteration

input Factor adjacency matrices $(\mathbf{U}, \mathbf{V}) \in \mathbb{R}^{d \times m} \times \mathbb{R}^{m \times d}$ and number of iterations $T \in \mathbb{N}$

- 1: Initialize $p_0 \in \mathbb{R}^d$ and $q_0 \in \mathbb{R}^d$, either randomly or by warm-starting with previous estimates of the leading singular vectors of \mathbf{UV}
- 2: **for** $t \in \{0, \dots, T - 1\}$ **do**
- 3: $p_{t+1} = \mathbf{V}^\top \mathbf{U}^\top p_t / \|\mathbf{V}^\top \mathbf{U}^\top p_t\|_2$
- 4: $q_{t+1} = \mathbf{UV} q_t / \|\mathbf{UV} q_t\|_2$

output Approximate leading singular value $\hat{\rho} = \frac{p_T^\top \mathbf{UV} q_T}{p_T^\top q_T}$

E Implementation details for DCD-FG

In this section, we present the implementation details for DCD-FG.

E.1 Factor MLP: Likelihood model and architecture details

For adjacency matrices \mathbf{U} and \mathbf{V} of the f -DiGraph G_f , we detail now how, for DCD-FG, we construct a likelihood model that is both non-linear and uses the factor semantics. We define h_f as a (deterministic) variable attached to factor node $f \in F$, calculated as the scalar output of a multi-layer perceptron (MLP) on the input variables of each factor defined by the matrix \mathbf{U} ,

$$h_f = \text{MLP}(\mathbf{U}_{:,f} \circ X; \Theta_f), \quad (72)$$

for neural networks parameters Θ_f , and $X \in \mathbb{R}^d$, where masking with \mathbf{U} is a computationally efficient way to restrict the input to the neural network to a potentially varying set of input variables. We provide the default hyperparameters for these MLPs in Appendix F. Further, we let the conditional distribution of each node depend linearly on its parent factors defined by the matrix \mathbf{V} ,

$$X_j \sim \text{Normal}(\alpha_j^\top (\mathbf{V}_{j,:} \circ h) + \beta_j, \sigma_j^2), \quad (73)$$

for parameters $\alpha_j \in \mathbb{R}^m$, $\beta_j \in \mathbb{R}$, $\sigma_j > 0$.

These equations correctly specify a density model $p_\Theta(X_j | X_{-j})$ as long as the obtained likelihood does not depend on feature X_j , but only on the other features X_{-j} . In particular, this is true for all j if $\text{diag}(\mathbf{UV}) = \mathbf{0}_{d \times d}$ (i.e., if there are no self-loops in G).

E.2 Linear model and relationship to NOTEARS-LR

We briefly explore connections between our factor architecture, and the NOTEARS-LR model [20]. In the context of our factor architecture with linear models, each factor variable h_f is a linear combination of X with weights $r_f \in \mathbb{R}^d$. Omitting bias terms for simplicity, we collect these weights into a matrix $\mathbf{R} = [r_1, \dots, r_m]$. Similarly, each feature X_j is a linear combination of h_f with weights $\alpha_j \in \mathbb{R}^m$ that we similarly condense into a matrix $\mathbf{A} = [\alpha_1, \dots, \alpha_d]$. In this case, the mean of our Gaussian conditional likelihood model can be written as

$$\mathbb{E}[X_j | X] = \mathbf{A}\mathbf{R}X. \quad (74)$$

Interestingly, without further modifications, we observed that this model suffers from misspecification, as well as poor performance due to the possibility of self-loops. In the linear case, a simple workaround to this problem is to mask contributions due to self-loops by removing the diagonal of the matrix $\mathbf{A}\mathbf{R}$. This corresponds to modifying the likelihood model to

$$\mathbb{E}[X_j | X] = \mathbf{M}_{\text{no-loop}} \circ (\mathbf{A}\mathbf{R})X, \quad (75)$$

where $\mathbf{M}_{\text{no-loop}} = \mathbb{1}\mathbb{1}^\top - \mathbf{I}_{d \times d}$ is a self-loop removing mask. This modification is exactly the linear model proposed by NOTEARS-LR. While this simple modification effectively eliminates self-loops, it necessitates expanding the full matrix $\mathbf{A}\mathbf{R}$, which incurs a runtime cost of $O(d^2)$. Next, we describe an alternative approach that avoids this step.

E.3 Removing self-loops in f -DAGs

Parametrizing the f -DAG adjacency matrix by $\mathbf{M} = [\mathbf{U}, \mathbf{V}]$ with otherwise unconstrained binary matrices \mathbf{U} and \mathbf{V} causes the induced feature graphs to potentially have a large number of self-loops. As emphasized before, this causes the local likelihood to not be correctly specified. We also found this to be detrimental to the performance of the model, even though the acyclicity score should promote the absence of self-loops in later stages of training. We hypothesize that when self-loops are present, the model starts off training by predicting every variable by itself, which in turn prevents any other signal from being picked up during the training stage. Therefore, the model never learns a meaningful predictive model that can be accurately pruned into a DAG.

To circumvent this issue, we propose an alternative model in which the matrices \mathbf{U} and \mathbf{V} are additionally constrained to explicitly remove self-loops. More precisely, we calculate $\mathbf{M} = [\mathbf{U}, \mathbf{V}]$ as a deterministic mapping from a single $d \times m$ matrix \mathbf{W} , taking value in $\{0, -1, 1\}^{d \times m}$ with independent entries sampled according to a Gumbel-softmax distribution [61] with parameters Φ .

The intuition behind this single matrix is that each individual entry \mathbf{W}_{ij} decides whether there is an edge between a factor f_j and a feature v_i , as well as its orientation. More precisely,

$$\forall i \in [d], j \in [m], (\mathbf{U}_{ij}, \mathbf{V}_{ji}) = \begin{cases} (1, 0), & \text{for } \mathbf{W}_{ij} = 1, \\ (0, 1), & \text{for } \mathbf{W}_{ij} = -1, \\ (0, 0), & \text{for } \mathbf{W}_{ij} = 0. \end{cases} \quad (76)$$

Because the entries \mathbf{U}_{ij} and \mathbf{V}_{ji} may never be both equal to 1, there are no self-loops in the induced half-square graph. Indeed, the number of self-loops is simply the trace of the adjacency matrix, which is equal to zero,

$$\text{Tr}(\mathbf{UV}) = \sum_{i=1}^d \sum_{j=1}^m \mathbf{U}_{ij} \mathbf{V}_{ji} = 0. \quad (77)$$

In the case of DCD-FG, it is important to notice that the matrices \mathbf{U} and \mathbf{V} are not fixed, but sampled from a random distribution $\mathbf{M}(\Phi)$ (we drop dependence to the parameter Φ for convenience of notation). For the purpose of later enforcing acyclicity, we calculate the expectation of the weighted (random) adjacency matrices formed from $\mathbf{M}(\Phi)$, which, by independence of the entries of \mathbf{W} , is

$$\forall i, j \in [d]^2, \mathbb{E}[\mathbf{UV}]_{ij} = \begin{cases} (\mathbb{E}[\mathbf{U}]\mathbb{E}[\mathbf{V}])_{ij}, & \text{for } i \neq j, \\ 0, & \text{for } i = j. \end{cases} \quad (78)$$

Analogously, the expectation of the adjacency matrix of the induced factor graph is

$$\forall k, \ell \in [m]^2, \mathbb{E}[\mathbf{VU}]_{k\ell} = \begin{cases} (\mathbb{E}[\mathbf{V}]\mathbb{E}[\mathbf{U}])_{k\ell}, & \text{for } k \neq \ell, \\ 0, & \text{for } k = \ell. \end{cases} \quad (79)$$

E.4 Acyclicity penalties

We now show how acyclicity penalties can be applied to our factored representations (tr-exp factor and spectral factor in the experiments), and that they have the claimed runtime bounds, i.e., that they are linear in d . For both the tr-exp and the spectral radius penalty, we apply the continuous acyclicity penalty $\mathcal{C}(\mathbb{E}[\mathbf{M}(\Phi)])$ to the expectation of $\mathbf{M}(\Phi) = [\mathbf{U}(\Phi), \mathbf{V}(\Phi)]$, as in [6]. We leave the investigation of instead calculating gradients of the expected penalty $\mathbb{E}[\mathcal{C}(\mathbf{M}(\Phi))]$ with respect to Φ using reparameterized samples of $\mathbf{M}(\Phi)$ as future work.

Tr-exp factor penalty We apply the tr-exp penalty to $\mathbb{E}[\mathbf{VU}]$, the weighted adjacency matrix on the half-square $G_f^2[F]$ induced by the factor nodes. As described above in (79), $\mathbb{E}[\mathbf{VU}]$ is calculated by calculating the matrix product of the expectations of \mathbf{V} and \mathbf{U} , before setting the diagonal to zero. This $m \times m$ matrix can be calculated in $O(m^2d)$, and the gradient of the penalty $h(\mathbb{E}[\mathbf{M}]) = \text{Tr exp}\{\mathbb{E}[\mathbf{VU}]\} - m$ can be calculated in $O(m^3)$, yielding a total runtime of $O(m^3 + m^2d)$.

Spectral radius factor penalty We apply the factor power iteration (Algorithm 1) to the matrix $\mathbb{E}[\mathbf{UV}]$ to maintain left and right eigenvectors for the leading singular value in $O(Tmd)$ operations, and then calculate the gradient of that singular value in time $O(md)$. In this case, we use a simple modification of Algorithm 1 with a diagonal offset, noticing that

$$\mathbb{E}[\mathbf{UV}] = \mathbb{E}[\mathbf{U}]\mathbb{E}[\mathbf{V}] - \text{diag}(\mathbb{E}[\mathbf{U}]\mathbb{E}[\mathbf{V}]), \quad (80)$$

and that the matrix-vector multiplications in Algorithm 1 can be calculated in time $O(md)$.

E.5 Augmented Lagrangian

This section is adapted from the supplementary materials of the work of Brouillard, Lachapelle et al. [6] and outlines how the DAG-constrained optimization problem can be solved with first-order methods.

Let us recall that the score function and the optimization problem for DCD-FG, assuming perfect interventions, are defined as:

$$\max_{\Phi, \Theta} \mathcal{S}(\Phi, \Theta) \text{ such that } \mathcal{C}(\mathbb{E}[\mathbf{M}(\Phi)]) = 0, \quad (81)$$

$$\text{where } \mathcal{S}(\Phi, \Theta) = \mathbb{E}_{\mathbf{M}' \sim \mathbf{M}(\Phi)} \left[\sum_{k=1}^K \mathbb{E}_{X \sim P^{\text{data}}(k)} \sum_{j \notin \mathcal{L}_k} \log p_{\Theta}^j(X_j; \mathbf{M}'_j, X_{-j}) \right] - \lambda \|\mathbb{E}[\mathbf{M}(\Phi)]\|_1. \quad (82)$$

The augmented Lagrangian transforms the constrained problem into a sequence of unconstrained problems of the form

$$\max_{\Phi, \Theta} \mathcal{S}(\Phi, \Theta) - \gamma_t \mathcal{C}(\mathbb{E}[\mathbf{M}(\Phi)]) - \frac{\mu_t}{2} (\mathcal{C}(\mathbb{E}[\mathbf{M}(\Phi)]))^2, \quad (83)$$

where γ_t and μ_t are the Lagrange multiplier and the penalty coefficient of the t -th unconstrained optimization problem, respectively. In all our experiments, we initialize $\gamma_0 = 0$ and $\mu_0 = 10^{-8}$. Each such problem is approximately solved using a first-order stochastic optimization procedure (RMSProp in our experiments). We assume that a subproblem has converged when (83) evaluated on a validation set stops increasing. Let (Φ_t^*, Θ_t^*) be the approximate solution to subproblem t . Then, γ_t and μ_t are updated according to the following rule:

$$\gamma_{t+1} = \gamma_t + \mu_t \mathcal{C}(\mathbb{E}[\mathbf{M}(\Phi_t^*)]) \quad (84)$$

$$\mu_{t+1} = \begin{cases} \eta \mu_t, & \text{if } \mathcal{C}(\mathbb{E}[\mathbf{M}(\Phi_t^*)]) > \delta \mathcal{C}(\mathbb{E}[\mathbf{M}(\Phi_{t-1}^*)]), \\ \mu_t, & \text{otherwise,} \end{cases} \quad (85)$$

with $\eta = 2$ and $\delta = 0.9$. Each subproblem t is initialized using the previous subproblem's solution $(\Phi_{t-1}^*, \Theta_{t-1}^*)$. The augmented Lagrangian procedure is stopped when $\mathcal{C}(\mathbb{E}[\mathbf{M}(\Phi_t^*)]) < 10^{-8}$, or $\mu_t > 10^{32}$.

The gradient of (83) with respect to the parameters Φ and Θ is estimated on a minibatch of observations. To compute the gradient of the likelihood part with respect to Φ , we follow [6] and use a Straight-Through Gumbel-Softmax estimator [61]. This approach relies on discrete Bernoulli samples at the forward pass, but uses the reparameterized samples of the Gumbel softmax distribution for the backward pass (with fixed temperature parameter $T = 1$).

E.5.1 Code Statement

We implemented DCD-FG in PyTorch, using the DCIDI codebase as a starting point. We extensively refactored and modified the original code (simulations, loss functions, training, evaluation) in order to scale to thousands of variables, and to accommodate the simulation of factor graphs. The software is available as open-source on GitHub at <https://github.com/Genentech/dcdfg> under the Apache 2.0 licence.

F Details for empirical evaluation of DCD-FG

In this section, we provide the necessary details for reproducing the experiments in the paper.

F.1 Synthetic data sets

For each type of synthetic data set, we first sampled an f -DAG as explained in Appendix B.3, with $p_v = 0.1$ and $p_f = 0.2$ and then we sampled the causal mechanisms, adapting the method from [6] as follows. In each of our half-square graphs ($d = 100$), and for each intervention regime $k \in [K]$, where $K = 100$, intervention targets with a size of 1 to 3 nodes were chosen uniformly at random. $n/(K + 1)$ independent observations were sampled for each interventional setting. The data were normalized, i.e., we subtracted the mean and divided by the standard deviation. In cases where IGSP

required feature aggregation, we clustered the features using spectral clustering as implemented by scikit-learn [62].

In the linear data sets, each node was set to be a linear function of its parent nodes (in the f -DAG), with additional Gaussian noise of standard deviation $\sigma = 0.4$. The coefficients were sampled uniformly from $[-1, -0.25] \cup [0.25, 1]$ (to make sure they are bounded away from zero). Interventions were handled by instead sampling the intervened-upon node from an isotropic Gaussian distribution with unit variance.

In the non-linear data sets (NN), each node was set to be a non-linear function of its parents nodes (in the f -DAG), with additional Gaussian noise of standard deviation $\sigma = 0.4$. The non-linear functions were fully-connected neural networks with one hidden layer of 20 units and hyperbolic tangent as nonlinearity in the hidden layer. The weights of each neural network were sampled from isotropic Gaussian distributions with unit variance. Similarly to the linear model, interventions were handled by instead sampling the intervened-upon node from an isotropic Gaussian distribution with unit variance.

F.2 Preprocessing of the Perturb-CITE-seq data set

We downloaded the data set from the Single Cell Portal of the Broad Institute (accession code SCP1064). We converted the data from log-normalized count per millions into raw counts for processing with the scanpy package [63]. We removed cell profiles with less than 500 expressed genes, and genes expressed in less than 500 cells. Then, we filtered the genes to include only the genetically-perturbed genes and the most variable genes for a total of $d = 1,000$ genes. We finally partitioned the cells from each of the three conditions (co-culture, IFN γ , and control) into distinct datasets. We used spectral clustering as implemented in sklearn for clustering, and selected three gene sets with 10, 20 and 50 modules.

F.3 Baseline Methods

In this section, we provide additional details on the baseline methods and cite the implementations that were used. NOTEARS [19] was extended to handle perfect interventions, and to use a Gaussian likelihood (with unequal variance across features). In contrast to the original implementation that used a second-order optimization method, the reimplementation used in this paper relies on first-order optimization. A similar GPU reimplementation was used in the NO-BEARS manuscript [26] and shown to be 100x faster for $d = 300$. NOTEARS-LR [20] and NOBEARS [26] were also reimplemented to handle interventions, and use a Gaussian likelihood.

We noticed floating point overflow in most experiments ($d > 100$) using 16 bit precision when calculating the tr-exp penalty. We first explored using 32 bit precision, but instead preferred scaling the matrix before computation of the penalty. We have noticed that using the spectral radius of the initialized adjacency matrix as scaling factor provided a nice safeguard, and have applied this throughout all the models.

Finally, we noticed that for the NOTEARS baseline, thresholding the weight matrix at $w^* = 0.3$ (as done in the original NOTEARS paper) provided poor performance on this benchmark, and in the biological dataset. Therefore, we adopted a single strategy for pruning the adjacency matrices into DAGs for all of NOTEARS, NOBEARS, NOTEARS-LR and DCD-FG. We threshold the weighted adjacency matrices (weights for NOTEARS, NOBEARS and NOTEARS-LR, and probabilities of edge for DCD-FG) where the threshold t^* is obtained by binary search with $T = 20$ evaluation of an (exact) acyclicity test to find the largest possible DAG for each method.

For IGSP, we used the implementation from <https://github.com/uhrerlab/causaldag>. The cutoff values used for `alpha-inv` was always the same as `alpha`. We used tools from the Python package Causal Discovery Toolbox [45] for calculating the SHD metrics.

F.4 Default hyperparameters and hyperparameter search

For all methods, we performed an exhaustive hyperparameter grid search. The models were trained on 80% observations and evaluated on 20% of the remaining ones (distinct interventions were used in the training and the held-out data used for evaluations). For all of NOTEARS, NOBEARS, NOTEARS-LR and DCD-FG, we searched over the regularization coefficient for sparsity λ . Additionally, for

NOTEARS-LR and DCD-FG, we searched over the number of learned factors m . For DCD-FG, we used the acyclicity penalty as a supplementary hyperparameter (spectral or trace of exponential). For IGSP, we scored the output by using it as a mask for fitting a linear model, and we explored several cutoff values `alpha` based on the value used in the original publication [7], and the best performing value in the experiments of [6]. Because IGSP did not terminate in many scenarios (after 5 hours, even with the Gaussian conditional independence), we ran the method in several instances of feature aggregation and observation subsampling and report the best performance. Feature aggregation means that we decreased the dimensionality of the dataset by summarizing the feature set into a cluster set by averaging all features within a cluster, and mapping intervention targets from the feature set to the cluster set. The complete hyperparameter search space for each algorithm is described in Table 2.

Table 2: Hyperparameter search spaces for each algorithm.

	Hyperparameter space
DCD-FG	$\log_{10}(\lambda) \in \{-3, -2, -1, 0, 1, 2\}$ $m \in \{10, 15, 20, 30, 50\}$ DAG penalty $\in \{\text{spectral, tr-exp}\}$
NOTEARS-LR	$\log_{10}(\lambda) \in \{-3, -2, -1, 0, 1, 2\}$ $m \in \{10, 15, 20, 30, 50\}$ DAG penalty $\in \{\text{spectral, tr-exp}\}$
NOTEARS	$\log_{10}(\lambda) \in \{-3, -2, -1, 0, 1, 2\}$ DAG penalty $\in \{\text{spectral, tr-exp}\}$
NOBEARS	$\log_{10}(\lambda) \in \{-3, -2, -1, 0, 1, 2\}$
IGSP	<code>alpha</code> $\in \{1e-3, 1e-5\}$ CI test $\in \{\text{Gaussian, KCI}\}$ Feature clustering (# clusters) $\in \{10, 20, 50\}$ Observation sub-sampling (only for bio dataset) $\in \{0.1, 0.25, 0.5\}$

DCD-FG, NOTEARS-LR, NOTEARS and NOBEARS share several default hyperparameters related to the optimization procedure and the architecture of the neural networks (for DCD-FG only) that we outline in Table 3 (values are similar to those in [6]). Neural networks were designed with leaky-ReLU activation functions, and initialized following the Xavier initialization [64]. RMSprop was used as the optimizer [65] with minibatches of size 64.

Table 3: Default hyperparameters for DCD-FG, NOTEARS, NOTEARS-LR and NOBEARS.

Hyperparameters
$\mu_0 = 10^{-8}, \gamma_0 = 0, \eta = 2, \delta = 0.9$
Augmented Lagrangian constraint threshold: 10^{-8}
Learning rate: $2 \cdot 10^{-3}$
hidden units: 16 (DCD-FG only)
hidden layers: 2 (DCD-FG only)

F.5 Assessment of statistical significance

For every claim of the form “Algorithm X and Y outperformed Algorithm W and Z with respect to metric h ”, we applied a Wilcoxon signed-rank test to the difference of scores between the worst performing model out of X, Y and the best performing model out of W, Z. We alternatively applied an Mann–Whitney U test (unpaired test) by concatenating the results of each algorithm (X, Y) and (W, Z) and recovered identical statistical significance assessments.

F.6 Additional experimental results

Here, we report the results of additional experiments intended to complement the experiments presented in the main paper and to investigate the robustness of DCD-FG:

- Aggregation of precision and recall on our Gaussian causal structural models, as presented in Figure 4, into a F1-score (Figure 7)
- Performance of DCD-FG for different values of the rank parameter (m) (Figure 8) on Gaussian causal structural models. For this, we considered the same data as for Figure 4, but performed hyperparameter search over all parameters besides m , for different choices of m . We observe that the performance is fairly robust to a wide variety of choices of m , and that validation likelihood is strongly correlated with the resulting performance, justifying our selection of m by optimizing hold-out likelihood.
- Alternative benchmark for a different exogeneous noise distribution (uniform instead of Gaussian; with matching variance; Figure 9). For this, we chose the same graph generative and conditional likelihood model as in Figure 4, only changing the noise distribution. While performance slightly degrades, the relative ordering of DCD-FG compared to NOTEARS-LR and NOTEARS remained the same.
- Alternative benchmark with observational data (Figure 10). Using the same graph generative and conditional likelihood model as in Figure 4, we generated the same number of observations, but without any interventions. Again, while performance decreases in this regime, DCD-FG remains the best-performig method.
- Total runtime of methods on all experiments (Figure 11).

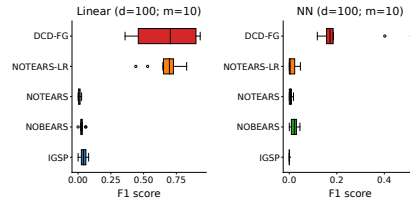


Figure 7: F1-score for Gaussian causal structural models experiments.

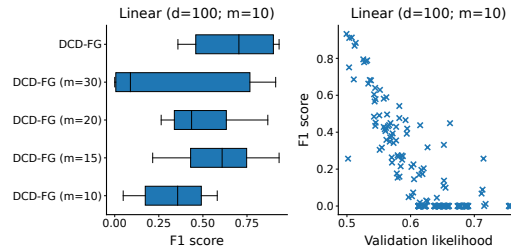


Figure 8: Robustness of DCD-FG to the rank hyperparameter.

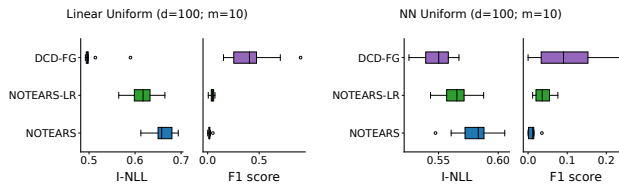


Figure 9: Robustness of DCD-FG to the model misspecification.

F.7 Biological interpretation of the f -DAG

The f -DAG inferred by DCD-FG for the cells treated with $\text{IFN}\gamma$ has $m = 20$ factors, and the half-square G has 196,303 edges. We show a histogram of ingoing and outgoing edges to each factor in Figure 12.

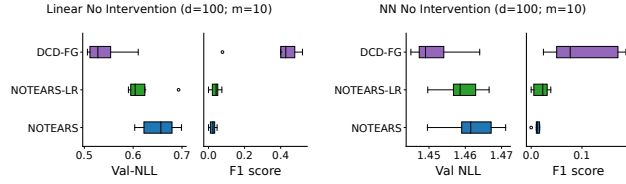


Figure 10: Performance of DCD-FG with observational data.

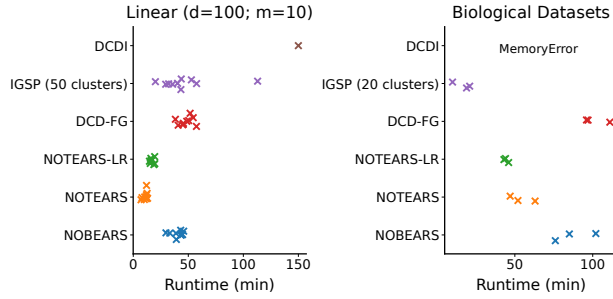


Figure 11: Total runtime of DCD-FG on one NVIDIA Tesla T4 GPU with 15Gb of RAM.

In order to assign biologically meaningful names to the factors, we performed Gene Set Enrichment Analysis (GSEA) via the `enrichr` method [50], applied independently to each factor f by considering the set of genes that are connected to f in either direction. In order to place the genes onto the factor half-square, we inferred for each gene the strongest factor-to-factor edge in which it appears. Indeed, we noticed that the same gene may appear upstream and/or downstream of several factors. For better interpretability, we selected the strongest parent factor and child factor based on the weights of the model (either the linear model in case of link from factor to gene, or the first layer of the MLP in case of link from gene to factor). We anticipate that further work will be necessary to visualize and interpret those large graphs for more involved biological applications, but we currently leave this as future work.

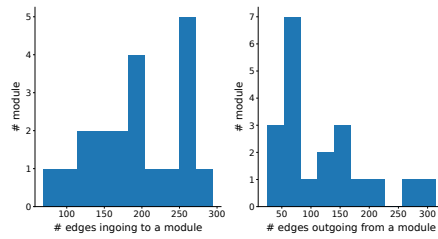


Figure 12: Distributions of ingoing and outgoing edges of modules in the f -DAG estimated on the IFN γ treated cells.